Kinetic Mechanism of Rat Polymerase β−dsDNA Interactions. Fluorescence Stopped-Flow Analysis of the Cooperative Ligand Binding to a Two-Site One-Dimensional Lattice†

Roberto Galletto, Maria J. Jezewska, and Wlodzimierz Bujalowski*

Department of Human Biological Chemistry and Genetics, Department of Obstetrics and Gynecology, Sealy Center for Structural Biology, and Sealy Center for Cancer Cell Biology, The University of Texas Medical Branch at Galveston, 301 University Boulevard, Galveston, Texas 77555-1053

Received June 22, 2004; Revised Manuscript Received October 28, 2004

ABSTRACT: Kinetics of cooperative binding of rat polymerase β to a double-stranded DNA has been studied using the fluorescence stopped-flow techniques. The data have been analyzed by an approach developed to examine complete kinetics of cooperative large ligand binding to a one-dimensional lattice. The method is based on using the smallest possible system that preserves key ingredients of cooperative binding; i.e., at saturation, the lattice can accept only two ligand molecules. It allows the identification of collective amplitudes as well as amplitudes describing particular normal modes of the reaction. The mechanism of the intrinsic binding of pol β to the dsDNA is different from the analogous mechanism for the ssDNA. The difference originates from different enzyme orientations in the corresponding complexes. Intrinsic binding to the dsDNA includes only two sequential steps: a very fast bimolecular association followed by an energetically favorable conformational transition of the complex. The transition following the bimolecular step does not facilitate the engagement of the enzyme in cooperative interactions. Its role seems to be reinforcing the affinity of the bimolecular step. Salt and magnesium cations affect both the bimolecular step and the conformational transition. As a result, the bimolecular step is less sensitive to the increased salt concentration, allowing the enzyme to preserve its initial dsDNA affinity. The changing character of cooperative interactions between bound enzyme molecules as a function of NaCl concentration and $MgCl_2$ concentration does not affect the binding mechanism. The engagement in cooperative interactions is ∼3−4 orders of magnitude slower than the conformational transition of the DNA-bound polymerase. The importance of the obtained results for the pol β activities is discussed.

Polymerase β (pol β) is one of a number of recognized DNA-directed polymerases in most eukaryotic cells that plays very specialized functions in the mammalian cell DNA repair machinery (*1*−*7*). A unique feature of a DNA repair polymerase including pol β is that the enzyme must recognize specific structures of damaged DNA sites. Moreover, the recognition of a damaged DNA site must precede chemical steps of the DNA synthesis. Among known specific activities of pol β are gap filling synthesis in mismatch repair, repair of monofunctional adducts, UV-damaged DNA, and abasic lesions in DNA (*1*−*7*). A DNA repair polymerase must be capable of specifically recognizing the common feature of damaged DNA sites, i.e., the presence of the single- and double-stranded (ss and ds, respectively) conformation of the nucleic acid. This capability is reflected in the structural organization of the total DNA-binding site of the enzyme and in mechanisms of interactions with the DNA (*8*−*12*).

The structure of pol β is a paradigm of the structure of the DNA repair polymerase (*7*). The enzyme possesses two functional domains, a large 31-kDa catalytic domain and a small 8-kDa domain, that constitute the total DNA-binding site (*8*−*12*). Both the 8- and 31-kDa domains have the ability to bind DNA; thus, the total DNA-binding site has two DNA-binding subsites (*8*−*12*). However, only the DNA-binding subsite on the 8-kDa domain of pol β has been found to have similar and significant affinity for both ss- and dsDNA (*12*, *13*). Thus, the subsite is the primary DNA-binding site of the enzyme. Moreover, its interactions with the DNA are specifically controlled by binding of Mg^{2+} cations to the domain (*12*). A similar organization of the enzyme molecule has been indicated for several other DNA polymerases engaged in DNA repair, although little is known about their nucleic acid binding mechanisms (*14*−*17*).

Interaction of human and rat pol β with the ssDNA is a very complex process, as already indicated by quantitative thermodynamic analyses (*8*−*12*). Both enzymes bind the ssDNA in two binding modes which differ in the number of occluded nucleotide residues, the $(\text{pol }\beta)_{16}$ and $(\text{pol }\beta)_5$ binding modes (*8*−*12*). In the $(\text{pol }\beta)_{16}$ binding mode, the total DNA-binding site of the enzyme is engaged in the complex; i.e., both the 8- and 31-kDa domains are involved in interactions with the ssDNA. In the $(\text{pol }\beta)_5$ binding mode, only the 8-kDa domain is engaged in interactions with the nucleic acid (*8*−*12*). Kinetic studies of interactions of human and rat pol β with the ssDNA, in the $(\text{pol }\beta)_{16}$ and $(\text{pol }\beta)_5$

† This work was supported by NIH Grant GM-58565 (to W.B.).

* To whom correspondence should be addressed: Department of Human Biological Chemistry and Genetics, The University of Texas Medical Branch at Galveston, 301 University Blvd., Galveston, TX 77555-1053. Telephone: (409) 772-5634. Fax: (409) 772-1790. E-mail: wbujalow@utmb.edu.

10.1021/bi0487037 CCC: $30.25
Published on Web 01/05/2005

binding modes, show that the binding mechanism is a complex multistep sequential reaction (*18*, *19*). The association is initiated through the very fast engagement of the DNA-binding subsite, located on the 8-kDa domain, in interactions with the nucleic acid. Analyses of the dynamics of gapped DNA recognition by both enzymes clearly indicate that the binding is also initiated through the 8-kDa domain (*20*). The ability of the 8-kDa domain to interact with the ss- and dsDNA is a key element in anchoring pol β to template-primer and gapped-DNA substrates (*10*−*12*). The 8-kDa domain binds to the ss- and/or dsDNA part of the gapped DNA downstream from the primer. The association of the 31-kDa domain with the dsDNA part of the gapped DNA substrate, containing the primer, follows the initial binding step.

Recent thermodynamic studies indicate that the binding of pol β to the dsDNA is very different from its interactions with the ssDNA or gapped DNA substrates (*21*). A peculiar aspect of the interactions of the enzyme with the dsDNA is the presence of significant cooperative interactions, dramatically controlled by the salt concentration and magnesium in solution. At low NaCl concentrations, the enzyme binds to the dsDNA with negative cooperativity, while at elevated salt concentrations and in the presence of magnesium, cooperativity is strong and positive. As a result, contrary to intrinsic affinities that are accompanied by a net ion release, cooperative interactions are accompanied by a net uptake of ions (*21*). Such behavior is very different from the salt effect on weak cooperative interactions between enzyme molecules in its binding modes on the ssDNA and gapped DNA, where little, if any, dependence upon salt has been found (*8*, *10*, *11*). Instead of different binding modes, the enzyme binds the dsDNA by forming a single type of complex with a site size (p) of 5 ± 1 bp. The small site size is a consequence of engagement of only the 8-kDa domain in intrinsic interactions with the dsDNA.

Elucidation of the interactions of pol β with the dsDNA is fundamentally important in understanding the molecular mechanism of the DNA recognition by the polymerase. Recall that although the enzyme binds to the specific structure of the damaged DNA site, it must recognize the site in the context of an overwhelming concentration of the dsDNA. Analysis of pol β−dsDNA interactions may also provide important general insights about the mechanisms of recognition of DNA substrates by other DNA repair polymerases. Despite its paramount importance for understanding the DNA recognition process, the direct analysis of the kinetics of the cooperative interactions of pol β with the dsDNA has not yet been quantitatively addressed.

In this paper, we report fluorescence stopped-flow kinetic analyses of the cooperative binding of rat pol β to the dsDNA. The obtained data have been analyzed using an approach developed to study complete kinetics of cooperative, large ligand binding to a one-dimensional lattice that, at saturation, can accept only two ligand molecules. Combined application of computer simulations and equilibrium data with examination of both relaxation times and amplitudes is essential for the approach. Intrinsic binding of pol β to the dsDNA includes only two sequential steps: very fast bimolecular association followed by an energetically favorable conformational transition of the complex. The transition following the bimolecular step does not facilitate the engagement in cooperative interactions. The changing character of cooperative interactions as a function of salt concentration and Mg^{2+} does not affect the mechanism of polymerase−dsDNA interactions. However, engagement in cooperative interactions is a slow process, ~3−4 orders of magnitude slower than conformational transition of the bound polymerase.

MATERIALS AND METHODS

Reagents and Buffers. All solutions were made with distilled and deionized >18 MΩ (Milli-Q Plus) water. All chemicals were reagent grade. Buffer C is 10 mM sodium cacodylate adjusted to pH 7.0 with HCl, 0.1 mM EDTA,[1] 1 mM DTT, and 10% glycerol. Temperatures and concentrations of salts in the buffer are indicated in the text.

Rat Pol β. Rat polymerase β was purified as previously described (*8*−*12*). The concentration of the protein was spectrophotometrically determined using an extinction coefficient (ϵ_{280}) of 2.1×10^4 cm^{-1} M^{-1} obtained with an approach based on Edelhoch's method (*8*−*12*, *22*, *23*).

Nucleic Acids. Modified and unmodified DNA oligomers were purchased from Midland Certified Reagents (Midland, TX). The labeled ssDNA oligomer contains a fluorescent label, 7-(diethylamino)-3-(4′-maleimidylphenyl)-4-methylcoumarin (CP), attached to the 5′ end through a six-carbon linker. Concentrations of all ssDNA oligomers have been spectrophotometrically determined as described previously by us (*24*−*26*). The dsDNA substrate was obtained by mixing the ssDNA oligomers at the given concentrations, warming the mixture for 5 min at 95 °C, and slowly cooling for a period of ~3−4 h (*24*−*26*). The melting temperature of the examined dsDNA oligomer is 54 ± 0.3 °C. The UV melting curve of the dsDNA 10-mer, used as a substrate in these studies, is included in the Supporting Information.

Fluorescence Measurements. Steady-state fluorescence measurements were performed using an SLM-AMINCO 8100C spectrofluorometer under magic angle conditions (*27*−*33*). Formation of the complex was followed by monitoring the fluorescence of the CP-labeled DNA (λ_{ex} = 435 nm, λ_{em} = 480 nm) (*21*). Computer fits were performed using KaleidaGraph (Synergy Software, Reading, PA) and Mathematica (Wolfram Research).

Stopped-Flow Kinetics. All fluorescence stopped-flow kinetic experiments were performed using an SX.18MV stopped-flow instrument (Applied Photophysics Ltd., Leatherhead, U.K.). The reactions were monitored by the dsDNA fluorescence, with a λ_{ex} of 435 nm. The emission was observed through a GG455 cutoff filter (Schott). Usually, five to eight traces were collected and averaged for each sample. The kinetic curves were fitted to extract relaxation times and amplitudes using the nonlinear least-squares software provided by the manufacturer, with the exponential function defined as

$$F(t) = F(\infty) + \sum_{i=1}^{n} A_i \exp(-\lambda_i t) \qquad (1)$$

[1] Abbreviations: DTT, dithiothreitol; EDTA, ethylenediaminetetraacetic acid, disodium salt; CP, 7-(diethylamino)-3-(4′-maleimidylphenyl)-4-methylcoumarin.

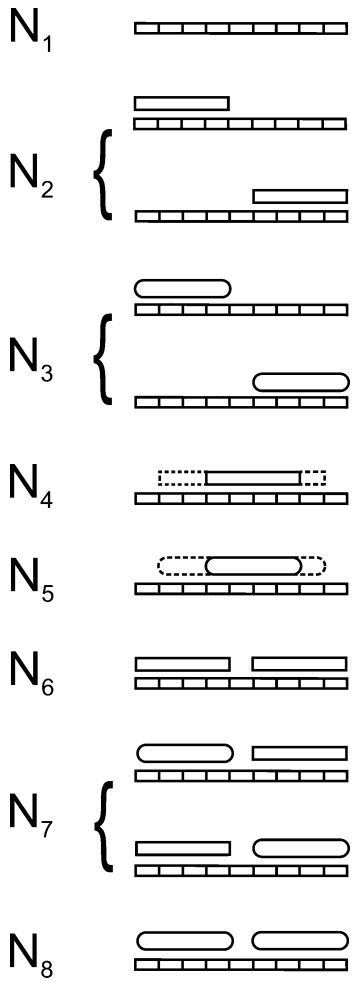

FIGURE 1: Schematic model of the cooperative large ligand binding to the one-dimensional lattice that, at saturation, can accept only two ligand molecules. The lattice contains 10 monomeric units (m), and the site size (p) of the ligand−lattice complex is 5 monomers. Due to the existence of potential binding sites, the first ligand can form complexes, N_2, that can still accept another ligand molecule, and complexes, N_4, where binding of another ligand is sterically prevented. There are four possible N_4 complexes initiated at different lattice sites. The dashed line symbolizes the range of these different locations. In states N_2 and N_4, the ligand undergoes a conformational transition following the binding step to form the N_3 and N_5 complexes, respectively. Association of the second molecule with N_2 and N_3 leads to the N_6 and N_7 species, respectively, that differ in the conformational states of the bound ligands; in these states, the ligand molecules are now engaged in cooperative interactions. In the N_8 complex, the bound molecules are in the final conformational state.

where $F(t)$ is the fluorescence intensity at time t, $F(\infty)$ is the fluorescence intensity at ∞ time, A_i is the amplitude corresponding to the ith relaxation process, λ_i is the time constant (reciprocal relaxation time) characterizing the ith relaxation process, and n is the number of relaxation processes.

RESULTS

Statistical Thermodynamic Model of Binding of Rat Pol β to the dsDNA 10-mer. The simplest extension of the statistical thermodynamic model of cooperative binding of a large ligand to a one-dimensional lattice that can accommodate, at saturation, only two ligand molecules is shown in Figure 1 (*21*). This model is analogous to the one used previously to analyze the binding of rat pol β to the dsDNA 10-mer, but includes an additional conformational transition of the bound ligand. The first ligand molecule can associate with the nucleic acid lattice, N_1, forming two types of complexes, N_2 and N_4, characterized by the same partial equilibrium constant, K_1. There are two complexes of the N_2 type that can still accept another ligand molecule with a site size (p) of 5. On the other hand, there are four N_4-type complexes, where the location of the bound ligand sterically prevents association of the second enzyme molecule. This is a characteristic situation in the case of the large ligand binding to a one-dimensional lattice, where instead of discrete sites, potential binding sites must be considered (*34*−*38*).

Both N_2 and N_4 undergo the same conformational transition to N_3 and N_5 complexes, respectively, described by the partial equilibrium constant K_2. The second ligand molecule can bind to the N_2 and N_3 complexes, forming the N_6 and N_7 complexes, respectively. These complexes differ in the conformational states of the two bound ligand molecules. Moreover, bound molecules are now engaged in cooperative interactions characterized by the cooperativity parameter, ω (*34*−*38*). Cooperative interactions between the enzyme molecules in different conformational states are taken to be identical. This assumption is justified by the equilibrium studies indicating that a single value of ω characterizes cooperative binding of rat pol β to the dsDNA (*21*). In the N_7 complexes, the enzyme molecules undergo a conformational transition to form the N_8 complex. The partition function, Z_m, describing the considered binding system is (*10*, *21*, *34*−*38*)

$$Z_m = 1 + (m - p + 1)K_1(1 + K_2)P_F + [K_1(1 + K_2)]^2\omega P_F^2 \quad (2)$$

where m is the total number of base pairs in the oligomer (10), p is the site size of the pol β−dsDNA complex (5), and P_F is the free pol β concentration. Comparison with the statistical thermodynamic model, used to analyze equilibrium binding isotherms of rat pol β to the same dsDNA oligomer lattice, indicates that the intrinsic binding constant K_{int}, obtained from equilibrium studies, is defined, in terms of the partial equilibrium constants, as (*21*)

$$K_{int} = K_1(1 + K_2) \quad (3)$$

The average degree of binding, $\sum\Theta_i$, the number of pol β molecules bound per DNA oligomer, is then

$$\sum\Theta_i = \frac{(m - p + 1)K_1(1 + K_2)P_F + 2[K_1(1 + K_2)]^2\omega P_F^2}{Z_m} \quad (4)$$

Analysis of Stopped-Flow Kinetic Experiments of the Cooperative Large Ligand Binding to a Two-Site One-Dimensional Lattice. The kinetic mechanism corresponding to the considered statistical thermodynamic model, depicted in Figure 1, is shown in Scheme 1. Despite applied simplifications in the formulation of the binding model, the kinetic mechanism is very complex. There are six rate parameters that describe the considered cooperative binding: k_1 and k_{-1}, characterizing the bimolecular step; k_2 and k_{-2}, characterizing the conformational transition of bound

Scheme 1

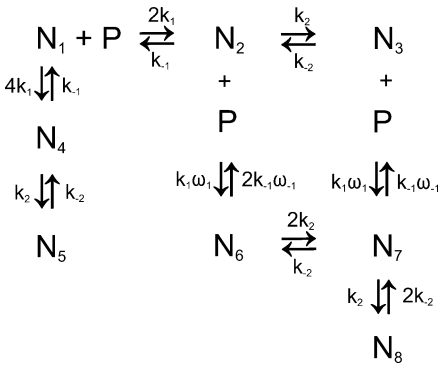

enzyme molecules; and ω_1 and ω_{-1}, association and dissociation cooperativity factors, respectively, resulting from the engagement in cooperative interactions. These rate parameters are related to the equilibrium binding parameters as follows: $K_1 = k_1/k_{-1}$, $K_2 = k_2/k_{-2}$, and $\omega = \omega_1/\omega_{-1}$. There are eight possible states of the dsDNA and eight steps in the mechanism. The same number of states and reaction steps results from the presence of the cyclic pathway, including N_2, N_3, N_6, and N_7 intermediates (Scheme 1) (*39*−*42*).

Quantitative analysis of spectroscopic stopped-flow measurements requires the examination of both the relaxation times and the amplitudes of the observed processes. In our studies, we used the matrix projection operator technique as we described previously (*40*−*43*). This powerful method is particularly useful for providing closed-form explicit expressions for amplitudes of the studied reaction (*40*−*42*). The kinetics of cooperative binding of pol β to the dsDNA is followed by changes in the fluorescence intensity of the nucleic acid (*21*). Differential equations describing the time course of the reaction described by Scheme 1, in terms of different dsDNA species, are

$$\frac{dN_1}{dt} = -6k_1PN_1 + k_{-1}N_2 + k_{-1}N_4 \quad (5a)$$

$$\frac{dN_2}{dt} = 2k_1PN_1 - (k_1\omega_1P + k_{-1} + k_2)N_2 + k_{-2}N_3 + 2k_{-1}\omega_{-1}N_6 \quad (5b)$$

$$\frac{dN_3}{dt} = k_2N_2 - (k_1\omega_1P + k_{-2})N_3 + k_{-1}\omega_{-1}N_7 \quad (5c)$$

$$\frac{dN_4}{dt} = 4k_1PN_1 - (k_{-1} + k_2)N_4 + k_{-2}N_5 \quad (5d)$$

$$\frac{dN_5}{dt} = k_2N_4 - k_{-2}N_5 \quad (5e)$$

$$\frac{dN_6}{dt} = k_1\omega_1PN_2 - (2k_{-1}\omega_{-1} + 2k_2)N_6 + k_{-2}N_7 \quad (5f)$$

$$\frac{dN_7}{dt} = k_1\omega_1PN_3 + 2k_2N_6 - (k_{-1}\omega_{-1} + k_2 + k_{-2})N_7 + 2k_{-2}N_8 \quad (5g)$$

$$\frac{dN_8}{dt} = k_2N_7 - 2k_{-2}N_8 \quad (5h)$$

Experiments described in this work were performed in a large excess of the polymerase over the nucleic acid, $P \gg N$; i.e., P is equal to the total concentration of the enzyme and is constant during the time course of the reaction. In matrix notation, system 5 is defined as

$$\begin{pmatrix} \frac{dN_1}{dt} \\ \frac{dN_2}{dt} \\ \frac{dN_3}{dt} \\ \frac{dN_4}{dt} \\ \frac{dN_5}{dt} \\ \frac{dN_6}{dt} \\ \frac{dN_7}{dt} \\ \frac{dN_8}{dt} \end{pmatrix} = \begin{pmatrix} -6k_1P & k_{-1} & 0 & k_{-1} & 0 & 0 & 0 & 0 \\ 2k_1P & -(k_1\omega_1P + k_{-1} + k_2) & k_{-2} & 0 & 0 & 2k_{-1}\omega_{-1} & 0 & 0 \\ 0 & k_2 & -(k_1\omega_1P + k_{-2}) & 0 & 0 & 0 & k_{-1}\omega_{-1} & 0 \\ 4k_1P & 0 & 0 & -(k_{-1} + k_2) & k_{-2} & 0 & 0 & 0 \\ 0 & 0 & 0 & k_2 & -k_{-2} & 0 & 0 & 0 \\ 0 & k_1\omega_1P & 0 & 0 & 0 & -(2k_{-1}\omega_{-1} + 2k_2) & k_{-2} & 0 \\ 0 & 0 & k_1\omega_1P & 0 & 0 & 2k_2 & -(k_{-1}\omega_{-1} + k_2 + k_{-2}) & 2k_{-2} \\ 0 & 0 & 0 & 0 & 0 & 0 & k_2 & -2k_{-2} \end{pmatrix} \begin{pmatrix} N_1 \\ N_2 \\ N_3 \\ N_4 \\ N_5 \\ N_6 \\ N_7 \\ N_8 \end{pmatrix} \quad (6)$$

and

$$\dot{\mathbf{N}} = \mathbf{M}\mathbf{N} \quad (7)$$

where $\dot{\mathbf{N}}$ is a vector of time derivatives, $\mathbf{M}$ is the coefficient matrix, and $\mathbf{N_0}$ is the vector of initial concentrations of different dsDNA species. To obtain the solution of system 6, we expand matrix $\mathbf{M}t$ using its eigenvalues, λ_i, and the projection operators, $\mathbf{Q}_i$, as (*38*−*40*)

$$\exp(\mathbf{M}t) = \sum_{i=0}^{8} \mathbf{Q}_i \exp(\lambda_i t) \quad (8)$$

The projection operators, $\mathbf{Q}_i$, can easily be analytically defined using the original coefficient matrix $\mathbf{M}$ and its eigenvalues, λ_i, by Sylvester's theorem (*40*−*43*). A general formula for a projection operator, $\mathbf{Q}_i$, corresponding to an eigenvalue, λ_i, is

$$\mathbf{Q}_i = \frac{\prod_{j \neq i}^{n} (\mathbf{M} - \lambda_j \mathbf{I})}{\prod_{j \neq i}^{n} (\lambda_i - \lambda_j)} \quad (9)$$

where n is the number of eigenvalues and $\mathbf{I}$ is the identity matrix that is the same size as $\mathbf{M}$.

In the considered mechanism depicted in Scheme 1 (eqs 5 and 6), there are eight eigenvalues (λ_0−λ_7). One eigenvalue ($\lambda_0 = 0$) requires that at very long times ($t \rightarrow \infty$) the system approach equilibrium. Application of the matrix projection operators provides the solution, for the system of differential equations (eq 6), as

$$\mathbf{N} = \mathbf{Q_0}\cdot\mathbf{N_0} + \mathbf{Q_1}\cdot\mathbf{N_0}\exp(\lambda_1 t) + \mathbf{Q_2}\cdot\mathbf{N_0}\exp(\lambda_2 t) + \mathbf{Q_3}\cdot\mathbf{N_0}\exp(\lambda_3 t) + \mathbf{Q_4}\cdot\mathbf{N_0}\exp(\lambda_4 t) + \mathbf{Q_5}\cdot\mathbf{N_0}\exp(\lambda_5 t) + \mathbf{Q_6}\cdot\mathbf{N_0}\exp(\lambda_6 t) + \mathbf{Q_7}\cdot\mathbf{N_0}\exp(\lambda_7 t) \quad (10)$$

where $\mathbf{Q}_i$ values are defined by eq 9.

There are seven normal modes of the reaction corresponding to relaxation times $\tau_1 = (-1/\lambda_1)$, $\tau_2 = (-1/\lambda_2)$, $\tau_3 = (-1/\lambda_3)$, $\tau_4 = (-1/\lambda_4)$, $\tau_5 = (-1/\lambda_5)$, $\tau_6 = (-1/\lambda_6)$, and $\tau_7 = (-1/\lambda_7)$ and seven amplitudes (A_1−A_7). Each individual amplitude contains a contribution from fluorescence intensities characterizing all dsDNA intermediates. In general, each intermediate may have different fluorescence properties. Therefore, there are eight molar fluorescence intensities

(F_1−F_8) characterizing the N_1−N_8 states of the dsDNA oligomer, respectively, free and in complexes with the polymerase. Using projection operators, the numerical analysis of the complex multistep reaction is reduced to finding only the eigenvalues of the original coefficient matrix **M** (*40*−*42*).

Relaxation Times. Examination of the relaxation times of the kinetic process, as a function of ligand concentration, constitutes the first and fundamental step in establishing the mechanism of the complex reaction and obtaining rate constants of particular elementary processes (*39*−*42*). The considered mechanism has seven relaxation times. Although quantitative analyses of such a complex mechanism would be prohibitively difficult, the behavior of the pol β−dsDNA system discussed below indicates general underlying principles and methodology that can be applied to simplify the analysis and quantitatively address the kinetics of the system. This is particularly true if the bimolecular steps, conformational transition of the bound enzyme and association accompanied by cooperative interactions, are largely separated on the time scale (see below).

We first consider the case in which there are negative cooperative interactions between the bound pol β molecules, i.e., $\omega = \omega_1/\omega_{-1} < 1$. For instance, such a situation occurs at low salt concentrations and in the absence of magnesium cations (*21*). Relaxation times are obtained by direct, numerical determination of eigenvalues λ_1−λ_7 of matrix **M** at a given total protein ligand concentration, using the following identities: $1/\tau_1 = -\lambda_1$, $1/\tau_2 = -\lambda_2$, $1/\tau_3 = -\lambda_3$, $1/\tau_4 = -\lambda_4$, $1/\tau_5 = -\lambda_5$, $1/\tau_6 = -\lambda_6$, and $1/\tau_7 = -\lambda_7$. The selected rate constants are as follows: $k_1 = 1 \times 10^9$ M^{-1}, $k_{-1} = 1 \times 10^4$ s^{-1}, $k_2 = 800$ s^{-1}, $k_{-2} = 80$ s^{-1}, $\omega_1 = 0.002$, and $\omega_{-1} = 0.01$ ($\omega = 0.2$). The concentration of the DNA lattice is selected to be 2×10^{-8} M, a typical value in a stopped-flow experiment with fluorescence detection (*18*, *19*, *40*−*42*, *44*, *45*).

For the selected value of k_1, the bimolecular step is close to being a diffusion-controlled one. However, both rate constants, k_1 and k_{-1}, are at least 1 order of magnitude larger than rate constants k_2 and k_{-2}, respectively, characterizing the following conformational transitions which, in turn, are orders of magnitude larger than ω_1 and ω_{-1}. As a result, the values of the four largest reciprocal relaxation times ($1/\tau_1$−$1/\tau_4$) are well above ~1000 s^{-1}; i.e., these relaxation processes are beyond the resolution of a typical stopped-flow experiment (data not shown). They characterize three different bimolecular steps, with and without the preceding conformational transition, and the fastest intramolecular transition in the association reactions of two ligand molecules, as depicted in Scheme 1. The remaining three reciprocal relaxation times ($1/\tau_5$−$1/\tau_7$) for the considered mechanism (Scheme 1) are shown in Figure 2a. Because of large differences between values of selected rate constants among elementary steps, the relaxation times differ significantly at any concentration of the ligand; i.e., the normal modes of the reaction are close to the "uncoupled" ones (*39*−*42*). The plots reach plateau values at high ligand concentrations. As a result, $1/\tau_5$−$1/\tau_7$ become independent of the ligand concentration at high ligand concentrations. Such behavior is characteristic for normal modes describing intramolecular transitions (*39*−*42*). In the considered example, it indicates that the three slower relaxation times

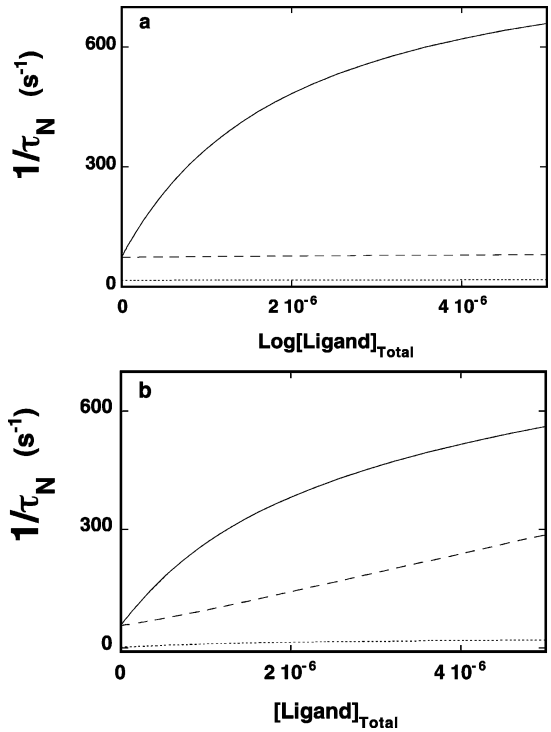

FIGURE 2: (a) Computer simulation of the dependence of individual reciprocal relaxation times [$1/\tau_5$ (—), $1/\tau_6$ (− − −), and $1/\tau_7$ (•••)] characterizing slow normal modes of the cooperative binding reaction, defined by Scheme 1, upon the total ligand concentration, for the case where there are negative cooperative interactions between bound ligand molecules. The simulations were performed with the following rate constants and cooperativity factors: $k_1 = 1 \times 10^9$ M^{-1} s^{-1}, $k_{-1} = 1 \times 10^4$ s^{-1}, $k_2 = 800$ s^{-1}, and $k_{-2} = 80$ s^{-1} and $\omega_1 = 0.002$ and $\omega_{-1} = 0.01$ ($\omega = 0.2$). (b) Computer simulation of the dependence of individual reciprocal relaxation times [$1/\tau_5$ (—), $1/\tau_6$ (− − −), and $1/\tau_7$ (•••)] characterizing slow normal modes of the cooperative binding reaction, defined by Scheme 1, upon the total ligand concentration, for the case where there are positive cooperative interactions between bound ligand molecules. The simulations were performed with the following rate constants and cooperativity factors: $k_1 = 1 \times 10^9$ M^{-1} s^{-1}, $k_{-1} = 1 \times 10^4$ s^{-1}, $k_2 = 600$ s^{-1}, and $k_{-2} = 60$ s^{-1} and $\omega_1 = 0.06$ and $\omega_{-1} = 0.001$ ($\omega = 60$). The concentration of the lattice in both panels is taken to be 2×10^{-8} M.

characterize the normal modes of intramolecular transitions, directly following the bimolecular step (τ_5) or occurring in a sequence of intramolecular steps (τ_6 and τ_7) (see below).

The situation is different for the case in which there are significant positive cooperative interactions. The selected rate constants are as follows: $k_1 = 1 \times 10^9$ M^{-1}, $k_{-1} = 1 \times 10^4$ s^{-1}, $k_2 = 600$ s^{-1}, and $k_{-2} = 60$ s^{-1}. Thus, the transition following the bimolecular step is only slightly slower than in the previously considered case (Figure 2a). The cooperative interaction factors are now $\omega_1 = 0.06$ and $\omega_{-1} = 0.001$, giving $\omega = 60$; i.e., there are strong positive cooperative interactions between bound ligand molecules. A large change in the cooperative interactions, by a factor of 300, has little effect on the largest reciprocal relaxation times ($1/\tau_1$−$1/\tau_4$) of the system (data not shown). This behavior is a simple consequence of the large separation of the relaxation processes on the time scale. Reciprocal relaxation times $1/\tau_5$−$1/\tau_7$, as a function of the total ligand concentration, are shown in Figure 2b. Comparison between computer simulations in panels a and b of Figure 2 shows that, contrary to the negative cooperativity case, relaxation time τ_6,

characterizing one of the slow normal modes related to the conformational transitions of the bound ligand, becomes much shorter and close to τ_5. Both relaxation times do not differ by more than a factor of ~2 over the examined ligand concentration range. In fact, for slightly larger values of ω_1 and ω_{-1}, the values of both relaxation times would be even closer (data not shown).

Amplitudes. Amplitudes of the spectroscopic relaxation process provide an additional test of the examined mechanism (*39*−*42*). Moreover, amplitudes determine which normal modes are observed and how they are observed in a stopped-flow experiment. The computer simulations have been performed using the molar fluorescence intensities selected: $F_1 = 1$, $F_2 = 2$, $F_3 = 2.3$, $F_4 = 2$, $F_5 = 2.3$, $F_6 = 3$, $F_7 = 3$, and $F_8 = 3$. Thus, the fluorescence intensity of the free nucleic acid is taken to be 1 (F_1). Complexes with a single bound ligand molecule are characterized by the same intensity ($F_2 = F_4 = 2$). The conformational transition is accompanied by an extra fluorescence change ($F_3 = F_5 = 2.3$). Complexes with two ligand molecules are characterized by the same fluorescence intensity ($F_6 = F_7 = F_8 = 3$). The rate constants are the same as in Figure 2a.

The dependence of amplitudes upon the logarithm of the total ligand concentration, for the mechanism depicted by Scheme 1, where there are negative cooperative interactions ($\omega = 0.2$), is shown in Figure 3a. The amplitudes are expressed as fractions of the total amplitude $A_{tot} = \sum A_i$, ($A_i/\sum A_i$) (*39*−*42*). First, for a given set of fluorescence and rate parameters, of four amplitudes characterizing the fast bimolecular steps, A_1−A_4, only the fastest process, characterized by A_1, contributes in a detectable way to the observed signal, although all intermediates contribute to the observed fluorescence (data not shown). Recall that all relaxation times of the fast normal modes are beyond the resolution of the stopped-flow measurement (see above). Therefore, in a stopped-flow experiment, all four amplitudes of the fast modes will appear as a single collective amplitude of the unresolved fast step, A_F. The observed collective amplitude of all fast steps is then defined as

$$A_F = A_1 + A_2 + A_3 + A_4 \qquad (11)$$

The collective amplitude A_F, as defined by eq 11, is shown in Figure 3a. It increases with an increase in ligand concentration. Second, the major contribution to the observed signal comes from amplitude A_5, characterizing one of the slow normal modes corresponding to the conformational transitions of the bound ligand molecules (Figure 3a). Because, for the considered negative cooperativity case, the relaxation times differ strongly in their values, the observed amplitude of the slow relaxation process in a stopped-flow experiment, A_5, will correspond to a given normal mode of the reaction; i.e., it will not be a collective amplitude. The amplitude, A_5, makes the major contribution to the observed signal. Notice that for the negative cooperative case ($\omega = 0.2$), the amplitude, A_6, is practically undetectable. The amplitude of the slowest mode, A_7, is barely visible; i.e., at most only two relaxation steps will be observed in the experiment (see below).

Similar to the behavior of the relaxation times, the behavior of amplitudes is different in the case of positive cooperative interactions. The dependence of fractional amplitudes upon the ligand concentration, for the considered mechanism, is shown in Figure 3b. The computer simulations have been performed using the same rate constants as in Figure 2b, i.e., $\omega_1 = 0.06$, $\omega_{-1} = 0.001$, and $\omega = 60$, and the same molar fluorescence intensities. As discussed above, four amplitudes characterizing the fast bimolecular steps are affected little by large positive cooperative interactions, with only the fastest process contributing significantly to the observed signal (data not shown). All these amplitudes will appear in a stopped-flow experiment as single collective

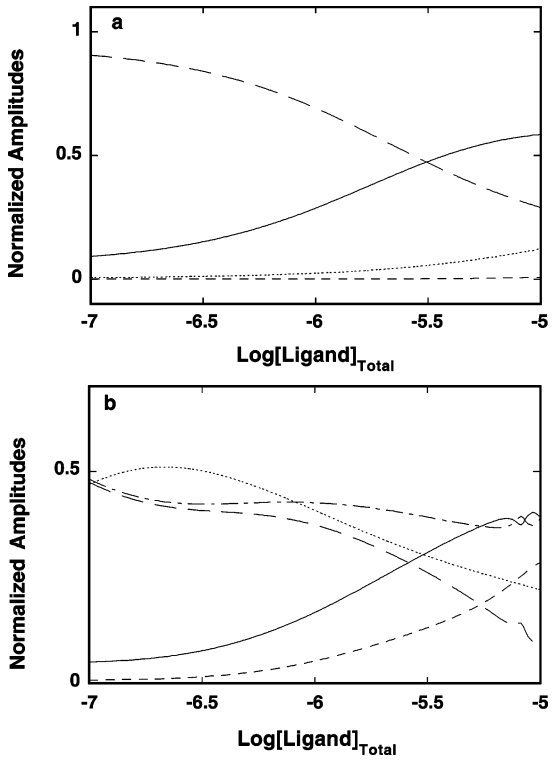

FIGURE 3: (a) Computer simulation of the dependence of relaxation amplitudes, for the cooperative binding reaction, defined by Scheme 1, upon the logarithm of the total ligand concentration, for the case where there are negative cooperative interactions between bound ligand molecules. The simulations were performed with the following rate constants and cooperativity factors: $k_1 = 1 \times 10^9$ M^{-1} s^{-1}, $k_{-1} = 1 \times 10^4$ s^{-1}, $k_2 = 800$ s^{-1}, and $k_{-2} = 80$ s^{-1} and $\omega_1 = 0.002$ and $\omega_{-1} = 0.01$ ($\omega = 0.2$). The relative fluorescence intensities ($F_2 = 2$, $F_3 = 2.3$, $F_4 = 2$, $F_5 = 2.3$, $F_6 = 3$, $F_7 = 3$, and $F_8 = 3$) characterize the corresponding intermediates (N_2−N_8, respectively). The molar fluorescence intensity of the free lattice, F_1, is taken to be 1, and the individual amplitudes are expressed as fractions of the total amplitude A_{Tot}. The collective amplitude that includes four fast normal modes of the reaction $A_F = A_1 + A_2 + A_3 + A_4$ (—), A_5 (− − −), A_6 (- - -), or A_7 (•••). (b) Computer simulation of the dependence of relaxation amplitudes, for the cooperative binding reaction, defined by Scheme 1, upon the logarithm of the total ligand concentration, for the case where there are positive cooperative interactions between bound ligand molecules. The simulations were performed with the following rate constants and cooperativity factors: $k_1 = 1 \times 10^9$ M^{-1} s^{-1}, $k_{-1} = 1 \times 10^4$ s^{-1}, $k_2 = 600$ s^{-1}, and $k_{-2} = 60$ s^{-1} and $\omega_1 = 0.06$ and $\omega_{-1} = 0.001$ ($\omega = 60$). The relative fluorescence intensities ($F_2 = 2$, $F_3 = 2.3$, $F_4 = 2$, $F_5 = 2.3$, $F_6 = 3$, $F_7 = 3$, and $F_8 = 3$) characterize the corresponding intermediates (N_2−N_8, respectively). The molar fluorescence intensity of the free lattice, F_1, is taken to be 1, and the individual amplitudes are expressed as fractions of the total amplitude A_{Tot}. The collective amplitude that includes four fast normal modes of the reaction $A_F = A_1 + A_2 + A_3 + A_4$ (—), A_5 (− − −), A_6 (- - -), or A_7 (•••). $A_{S2} = A_5 + A_6$ (− - −). The concentration of the lattice in both panels is taken to be 2×10^{-8} M.

amplitude, A_F, of the fast, unresolved process, shown in Figure 3b. The major contribution to the observed signal comes from amplitudes A_5-A_7 of the slow normal modes related to the conformational transitions. However, now the values of the relaxation time, τ_6, are close to τ_5 (Figures 2b and 3b). Therefore, in practice, a fitting routine will record these two normal modes as a single relaxation process. As a result, in a stopped-flow experiment, both normal modes, characterized by A_5 and A_6, will appear as a single normal mode with the amplitude A_{S1} ($=A_5 + A_6$). The collective amplitude A_{S1} is included in Figure 3b. On the other hand, amplitude A_7 describes the process with relaxation time τ_7 that is still much longer than any other relaxation time. In other words, A_7 corresponds strictly to the slowest normal mode of the reaction. However, contrary to the negative cooperativity case, A_7 will make a large contribution to the observed total relaxation process (Figure 3b). The increased contribution of the slowest relaxation process becomes a signature of the enhanced positive cooperative interaction in the examined system (see below).

Negative Cooperativity Case for Kinetics of the Cooperative Binding of Rat Pol β to the dsDNA. Equilibrium thermodynamic studies showed that binding of rat pol β to the dsDNA is characterized by significant cooperative interactions (*21*). As pointed out above, a peculiar aspect of these cooperative interactions is their very strong dependence upon the salt concentration and magnesium cations in solution. At low salt concentrations ([NaCl] < 100 mM), the cooperativity parameter ω is less than 1, indicating negative cooperative interactions. Conversely, at higher salt concentrations, ω becomes significantly larger than 1, particularly in the presence of magnesium cations, indicating strong positive cooperative interactions between the bound polymerase molecules (*21*).

To address the kinetics of the cooperative binding of pol β to the dsDNA, we first examined the enzyme binding at low salt concentrations and in the absence of Mg^{2+}, where cooperative interactions are negative, i.e., $\omega < 1$. Binding of rat pol β to the dsDNA is not accompanied by changes in protein fluorescence that are sufficiently large to allow us to examine complex binding or kinetic processes. However, we have found that association of the enzyme with a dsDNA oligomer labeled at the 5′ end of one of the ssDNA strands with the coumarin derivative, CP, is accompanied by a strong (~150%) increase in nucleic acid fluorescence, providing an excellent signal for monitoring the polymerase−dsDNA interactions (*21*). Moreover, the introduced label does not affect to any detectable extent the energetics of enzyme binding (*21*). As in our thermodynamic analyses of the polymerase interactions with the dsDNA, we selected the same dsDNA 10-mer, containing random sequences of bases, for the kinetic studies. The selected DNA substrate is depicted in Figure 4. Because the site size (p) of the enzyme−dsDNA complex is 5 bp, the selected oligomer can accept only two pol β molecules (*21*). Moreover, the dsDNA oligomer allows us to perform studies over large DNA and protein concentration ranges, avoiding the precipitation of the sample (*21*).

The stopped-flow kinetic traces of the dsDNA oligomer fluorescence, after mixing 1.5×10^{-8} M oligomer with several rat pol β concentrations in buffer C (pH 7.0, 10 °C), containing 50 mM NaCl, are shown in Figure 5. The initial

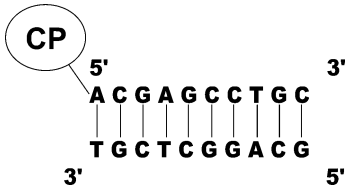

FIGURE 4: Primary structure of the dsDNA 10-mer used to examine the dynamics of interactions of rat pol β with the dsDNA. The nucleic acid has a coumarin derivative, CP, attached to the 5′ end of one of the ssDNA strands that provides the signal for monitoring the polymerase binding (*21*).

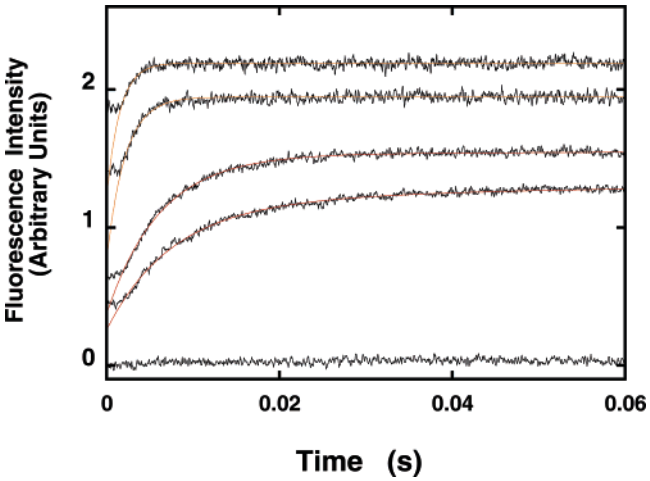

FIGURE 5: Set of fluorescence stopped-flow kinetic traces, after mixing the dsDNA 10-mer with rat pol β in buffer C (pH 7.0, 10 °C), containing 50 mM NaCl ($\lambda_{ex} = 435$ nm, $\lambda_{em} > 455$ nm). The final concentration of the nucleic acid 10-mer is 1.5×10^{-8} M oligomer, and the polymerase concentrations are 0, 7.6×10^{-8}, 1.2×10^{-7}, 6×10^{-7}, and 1.2×10^{-6} M from the bottom to the top. The solid brown and red lines are the one- and two-exponential, nonlinear least-squares fits of the experimental curves, respectively, using eq 1. The horizontal, initial part of each trace is the steady-state value of the fluorescence of the sample recorded 2 ms before the flow stopped. The trace at the bottom of the panel is the zero line obtained after mixing the nucleic acid, at the same concentration that was used with the enzyme, but with only the buffer.

~2 ms horizontal part of the traces corresponds to the steady-state fluorescence intensity recorded for 2 ms before the flow stops. The observed kinetics is complex. At lower enzyme concentrations, the two-exponential function (eq 1) provides an excellent description of the experimental traces. At higher enzyme concentrations, the traces are described by a one-exponential function. Including additional exponents does not improve the statistics of the fit (data not shown). The solid lines in Figure 5 are nonlinear least-squares fits with the indicated number of exponents. It should be pointed out that experiments performed under reversed pseudo-first-order conditions, i.e., in excess nucleic acid, showed the same number of relaxation times (data not shown). As we previously discussed, such behavior provides very strong evidence that the protein does not undergo any detectable conformational transition prior to the nucleic acid binding (*42*). The kinetics of binding of pol β to the dsDNA is very fast (*18*−*20*). The entire kinetic process takes less than ~200 ms to reach equilibrium, even at low enzyme concentrations.

The trace at the bottom in Figure 5 corresponds to the nucleic acid alone at the same concentration used with the protein but mixed with only the buffer (zero line). It is evident that the theoretical fits, although providing an

excellent description of the observed traces, do not account for the total fluorescence increase resulting from complex formation. The difference between the fluorescence intensity of the end point of the kinetic trace and the zero line recorded for the nucleic acid alone is the total amplitude of the reaction, A_{Tot} (*18*−*20*). Thus, regardless of any reaction mechanism, the stopped-flow data indicate that there is at least one additional fast step(s) preceding the observed kinetic processes, characterized by the relaxation time(s), which is too short to be extracted in the stopped-flow experiment. In other words, the cooperative association of rat pol β with the dsDNA is a process that includes at least three steps.

The two resolved reciprocal relaxation times, $1/\tau_{S2}$ and $1/\tau_{S3}$, obtained from the experimental traces, as a function of the total rat pol β concentration, are shown in Figure 6a. The values of $1/\tau_{S2}$ show a hyperbolic dependence upon the rat pol β concentration tending toward a plateau at high enzyme concentrations. The value $1/\tau_{S3}$ is detectable only in a limited concentration range (see above). Nevertheless, the value of $1/\tau_{S3}$ is very low compared to $1/\tau_{S2}$ and shows little dependence upon enzyme concentration, in the examined concentration range (Figure 6a). Such behavior indicates that both relaxation times must characterize intramolecular transitions of the formed complexes (*39*−*42*). In other words, the behavior of both slow relaxation times provides evidence that the enzyme−dsDNA complex undergoes an intramolecular conformational change following the binding step.

Equilibrium data show that under the solution conditions that were examined and in the pol β concentration range that was examined two polymerase molecules associate with the dsDNA (*21*). As discussed above, the simplest and minimum mechanism of cooperative binding of a large ligand to a one-dimensional lattice containing two binding sites, which can account for the observed unresolved fast process(s) and slow intramolecular transitions, is defined in Figure 1 and Scheme 1. Because the kinetic data clearly show that the bimolecular step is very fast, it must equilibrate well before the intramolecular conformational transitions proceed. Thus, the observed unresolved process contains all four fast normal modes characterized by $\tau_1-\tau_4$ (Figures 2 and 3). Therefore, the bimolecular step can be characterized by only its partial equilibrium constant, K_1. There are still five parameters in Scheme 1 that have to be determined. However, we can utilize the fact that we know the intrinsic binding constant K_{int}, from the equilibrium studies, which is related to partial equilibrium constants K_1 and K_2 by eq 3. Using the value of K_{int} reduces the number of parameters to four.

We applied the following strategy for the data analysis. The analysis is started by first simultaneously fitting both individual relaxation times $1/\tau_{S2}$ and $1/\tau_{S3}$ to obtain initial values of K_1, k_2, k_{-2}, ω_1, and ω_{-1}. Then, the behavior of the reciprocal relaxation times, $1/\tau_5-1/\tau_7$, is simulated using the obtained rate parameters. The corresponding computer simulations are shown in Figure 6b, indicating that relaxation times $\tau_5-\tau_7$ of the slow normal modes differ significantly in their values. Also, these data indicate that the experimentally observed relaxation times, τ_{S2} and τ_{S3}, correspond to relaxation times τ_5 and τ_7 of the normal modes of the reaction, respectively. Thus, the normal mode characterized by τ_6 must be undetectable in the stopped-flow data; i.e., it

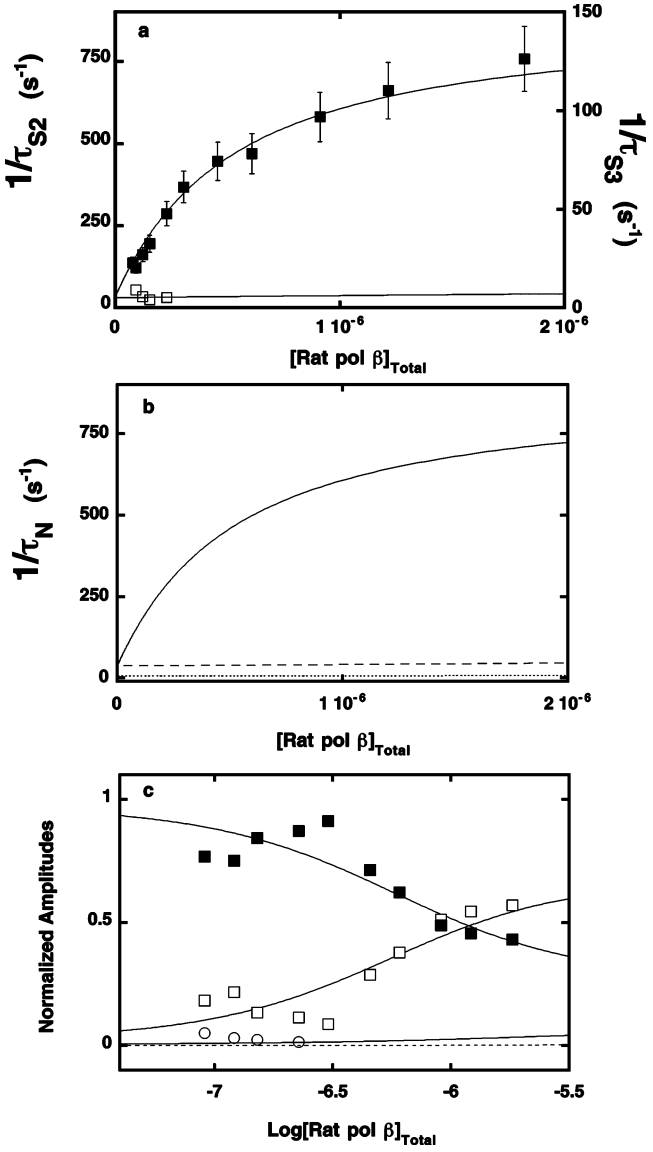

FIGURE 6: (a) Dependence of the reciprocal relaxation times, $1/\tau_{S2}$ (■) and $1/\tau_{S3}$ (□), for the binding of rat pol β to the dsDNA 10-mer, in buffer C (pH 7.0, 10 °C), containing 50 mM NaCl, upon the total concentration of the enzyme. The solid lines are nonlinear least-squares fits according to the mechanism, defined by Scheme 1, with the following rate constants and cooperativity factors: $K_1 = 1.06 \times 10^6$ M^{-1}, $k_2 = 838$ s^{-1}, and $k_{-2} = 44$ s^{-1} and $\omega_1 = 0.004$ and $\omega_{-1} = 0.014$ (details in the text). The error bars are standard deviations obtained from three to four independent experiments. (b) Computer simulation of the reciprocal relaxation times, $1/\tau_5-1/\tau_7$, corresponding to slow normal modes of the reaction defined by Scheme 1, using kinetic parameters obtained from the fit of experimental relaxation times, $1/\tau_{S2}$ and $1/\tau_{S3}$ (details in the text): $1/\tau_5$ (—), $1/\tau_6$ (− − −), and $1/\tau_7$ (···). (c) Dependence of experimental relaxation amplitudes, for the binding of rat pol β to the dsDNA 10-mer in buffer C (pH 7.0, 10 °C), containing 50 mM NaCl, upon the total concentration of the enzyme. The solid lines are computer fits according to the cooperative binding mechanism, defined by Scheme 1, with the following relative fluorescence intensities: $F_2 = 1.5$, $F_3 = 2.5$, $F_4 = 2.35$, $F_5 = 2.5$, $F_6 = 2.6$, $F_7 = 2.6$, and $F_8 = 2.6$. The maximum fluorescence increase of the nucleic acid is taken from the equilibrium fluorescence titration under the same solution conditions as the ΔF_{max} of 1.6 ± 0.15 (details in the text). The rate constants are the same as in panel a. The collective amplitude that includes four fast normal modes of the reaction $A_F = A_1 + A_2 + A_3 + A_4$ (□), A_5 (■), or A_7 (○). The dashed line is the theoretical dependence of amplitude A_6 upon the rat pol β concentration, obtained for the determined rate and spectroscopic parameters (Table 1).

must be characterized by a very low, if any, amplitude (see below).

As we pointed out above, relaxation times for the fast normal modes are beyond the resolution of the stopped-flow experiment. Therefore, all four amplitudes of the fast normal modes appear in a stopped-flow experiment as a single collective amplitude of the unresolved fast process (Figure 3a,b). This collective amplitude of all fast normal modes, A_F, can be obtained from the known amplitudes of the observed processes, A_{S2} and A_{S3}, and the total amplitude of the reaction as

$$A_F = A_{Tot} - A_{S2} - A_{S3} \quad (11a)$$

Because we already know that $A_{S2} = A_5$ and $A_{S3} = A_7$, the collective fast amplitude is, in the considered case, defined as

$$A_F = A_{Tot} - A_5 - A_7 \quad (11b)$$

The dependence of the normalized amplitudes (A_F, A_5, and A_7) upon the rat pol β concentration is shown in Figure 6c. At a low pol β concentration, amplitude A_5 dominates the observed signal, and it decreases with the increase in pol β concentration. As the pol β concentration increases, the collective amplitude of the fast processes, A_F, increases and becomes a dominant relaxation effect at high enzyme concentrations. Values of amplitude A_7 are low and only available over a limited enzyme concentration range.

There are eight possible different states of the dsDNA in the considered kinetic mechanism (Scheme 1). Because only two relaxation times and three amplitudes are available from the experiment, estimation of molar fluorescence parameters characterizing each intermediate requires additional, extra-kinetic information, which is provided by the equilibrium studies (*21*). First, the equilibrium data indicate that binding of a single pol β molecule to the dsDNA oligomer is accompanied by a factor of ~2 average increase in the nucleic acid fluorescence, while association of the second molecule induces a further factor of ~1.6 average fluorescence increase. Second, the initial dependence of the relative fluorescence increase of the nucleic acid, ΔF, upon the average degree of binding, $\sum\Theta_i$, is very close to a linear function, indicating that complexes N_2−N_5 are characterized by similar molar fluorescence intensities (*21*). The dependence of the relative fluorescence increase of the nucleic acid, ΔF, upon the average degree of binding, $\sum\Theta_i$, for $\sum\Theta_i$ values between 1 and 2 is also a linear function, strongly suggesting that protein−nucleic acid complexes containing two polymerase molecules are characterized by similar molar fluorescence intensities. Third, estimation of the molar fluorescence intensities of different intermediates is further facilitated by the fact that the maximum, fractional increase in the nucleic acid fluorescence ($\Delta F_{max} = 1.6 \pm 0.15$) is also known from equilibrium titrations (*21*). The value of ΔF_{max} can be analytically expressed as

$$\Delta F_{max} = \frac{\Delta F_6 + \Delta F_7 \times 2K_2 + \Delta F_8 K_2^2}{1 + 2K_2 + K_2^2} \quad (12)$$

where ΔF_6 [$=(F_6 - F_1)/F_1$], ΔF_7 [$=(F_7 - F_1)/F_1$], and ΔF_8 [$=(F_8 - F_1)/F_1$] are fractional fluorescence intensities of each intermediate in the association reaction of rat pol β with the dsDNA, relative to the molar fluorescence intensity of the free nucleic acid, F_1. Equation 12 provides an additional relationship among the fluorescence parameters, with the value of ΔF_{max} being a scaling parameter.

Therefore, the amplitude analysis begins with assignment of the initial values of the molar fluorescence intensities to the complexes as follows: $F_1 = 1$, $F_2 = 2$, $F_3 = 2.3$, $F_4 = 2$, $F_5 = 2.3$, $F_6 = 2.6$, $F_7 = 2.6$, and $F_8 = 2.6$. The computer simulations are then initiated by allowing the molar fluorescence intensities to float within ±30% of the initial values. In the final step of the analysis, global fitting, which simultaneously includes relaxation times and amplitudes, refines the values of the rate constants and molar fluorescence parameters. The solid lines in panels a and c of Figure 6 are computer fits of the relaxation times and amplitudes, according to the mechanism depicted in Scheme 1. These fits were performed using the optimal single set of spectroscopic and rate parameters that describe both the relaxation times and the amplitudes (*39*−*42*). A computer simulation of amplitude A_6 is also included in Figure 6c (dashed line). Its values are very low in the range of ~1% of the observed signal in the examined enzyme concentration range, making the process practically undetectable in the stopped-flow experiment, as pointed out above. The obtained rate constants and relative molar fluorescence intensities of all intermediates for the mechanism, defined by Scheme 1, are included in Table 1.

The partial equilibrium binding constant for the bimolecular step is K_1 [$(1.1 \pm 0.3) \times 10^6$ M^{-1}], indicating that the bimolecular step makes a predominant contribution to the free energy of the enzyme binding to the dsDNA. The forward and backward rate constants for the conformation transition, in the examined solution conditions, are as follows: $k_2 = 838 \pm 65$ s^{-1} and $k_{-2} = 44 \pm 12$ s^{-1}, providing $K_2 = 18.9 \pm 9$. Thus, the conformational transition of the bound pol β leads to a significantly increased affinity of the enzyme for the dsDNA. On the other hand, the cooperativity factors are ($\omega_1 = 0.004 \pm 0.001$ and $\omega_{-1} = 0.014 \pm 0.003$) dramatically lower than the rate parameters characterizing the conformational transition. The obtained value of $\omega = \omega_1/\omega_{-1} = 0.29 \pm 0.14$. This value is in good agreement with the ω value of 0.31 ± 0.06 obtained in equilibrium studies, indicating that binding of pol β to the dsDNA, at low salt concentrations ([NaCl] < 0.1 M), is characterized by negative cooperativity (*21*).

Under the studied solution conditions, the molar fluorescence intensities of all intermediates are within approximately ≤30% of their initial values, based on the analysis of equilibrium data (see above). Thus, the obtained results indicate that the conformational transition following the binding of the enzyme to the dsDNA is, with the exception of the N_2 intermediate, accompanied by a moderate additional fluorescence change of the complex, as reflected in similar values of F_3−F_5 characterizing the N_3−N_5 intermediates, respectively (Figure 1). Such effects on the nucleic acid fluorescence strongly suggest that the transition is, predominantly, a conformational change in the bound enzyme, including only a slight change in the structure of the nucleic acid. By the same token, similar values of the fluorescence intensities of intermediates containing two bound enzyme molecules indicate that cooperative interactions have little

Table 1: Kinetic, Thermodynamic, and Spectroscopic Parameters Characterizing the Cooperative Binding of Rat Pol β to the dsDNA 10-mer, in Buffer C (pH 7, 10 °C), Containing Different NaCl Concentrations

[NaCl] (mM)	K_1 (M^{-1})	k_2 (s^{-1})	k_{-2} (s^{-1})	ω_1	ω_{-1}	K_2	ω	K_{int} (M^{-1})	F_2^a	F_3^a	F_4^a	F_5^a	F_6^a	F_7^a	F_8^a
50	$(1.1 \pm 0.3) \times 10^6$	838 ± 65	44 ± 12	0.004 ± 0.001	0.014 ± 0.003	18.9 ± 9	0.29 ± 0.14	$(2.1 \pm 0.7) \times 10^7$	1.5 ± 0.1	2.5 ± 0.1	2.4 ± 0.1	2.5 ± 0.1	2.6 ± 0.1	2.6 ± 0.1	2.6 ± 0.1
75	$(2.7 \pm 1) \times 10^5$	878 ± 65	80 ± 18	0.015 ± 0.005	0.015 ± 0.005	11 ± 5	1 ± 0.4	$(3.2 \pm 1.1) \times 10^6$	0.8 ± 0.05	2.1 ± 0.1	2.1 ± 0.1	2.4 ± 0.1	2.7 ± 0.1	2.7 ± 0.1	2.5 ± 0.1
100	$(1.3 \pm 0.5) \times 10^5$	770 ± 40	112 ± 20	0.024 ± 0.004	0.012 ± 0.002	6.9 ± 2.5	2 ± 1	$(1.05 \pm 0.3) \times 10^6$	1.7 ± 0.1	2.4 ± 0.1	1.7 ± 0.1	1.9 ± 0.1	2.3 ± 0.1	2.3 ± 0.1	2.5 ± 0.1
150	$(8 \pm 1.6) \times 10^4$	835 ± 50	135 ± 25	0.05 ± 0.01	0.005 ± 0.001	6.1 ± 2.3	10 ± 4.2	$(4.0 \pm 1.3) \times 10^5$	2 ± 0.1	2.8 ± 0.1	1.9 ± 0.1	2.2 ± 0.1	2.6 ± 0.1	2.6 ± 0.1	2.3 ± 0.1

[a] Values relative to the fluorescence ($F_1 = 1$) of the free dsDNA 10-mer (details in the text).

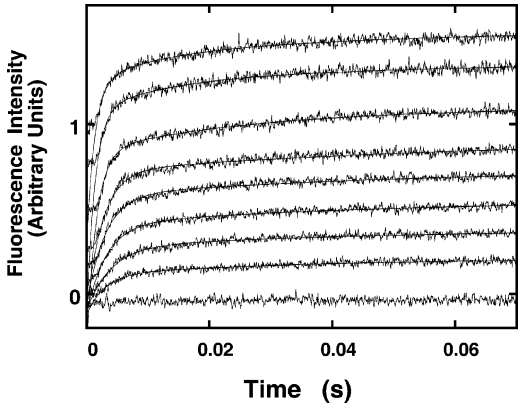

FIGURE 7: Set of fluorescence stopped-flow kinetic traces, after mixing the dsDNA 10-mer with rat pol β in buffer C (pH 7.0, 10 °C), containing 100 mM NaCl and 1 mM $MgCl_2$ ($\lambda_{ex} = 435$ nm, $\lambda_{em} > 455$ nm). The final concentration of the nucleic acid 10-mer is 1.5×10^{-8} M oligomer, and the polymerase concentrations are 0, 1.14×10^{-7}, 2.27×10^{-7}, 3.79×10^{-7}, 5.3×10^{-7}, 7.57×10^{-7}, 1.14×10^{-6}, 1.89×10^{-6}, and 3.6×10^{-6} M from the bottom to the top. The solid lines are the two-exponential, nonlinear least-squares fits of the experimental curves, using eq 1. The horizontal, initial part of each trace is the steady-state value of the fluorescence of the sample recorded 2 ms before the flow stopped. The trace at the bottom is the zero line obtained after mixing the nucleic acid, at the same concentration that was used with the enzyme, but with only the buffer.

effect on the conformation of the nucleic acid (Table 1). These data strongly suggest that cooperative interactions reflect, predominantly, protein−protein interactions between the bound polymerase molecules (see the Discussion).

Positive Cooperativity Case for Kinetics of the Cooperative Binding of Rat Pol β to the dsDNA. At higher salt concentrations, the cooperativity parameter, ω, becomes significantly larger than 1, particularly in the presence of Mg^{2+} cations, indicating strong positive cooperative interactions between the bound polymerase molecules (*21*). To address the kinetics of the binding of pol β to the dsDNA characterized by strong positive cooperative interactions, we examined the enzyme binding at elevated salt concentrations and in the presence of magnesium. The stopped-flow kinetic traces of the dsDNA oligomer fluorescence, after mixing 1.5×10^{-8} M DNA oligomer with several rat pol β concentrations in buffer C (pH 7.0, 10 °C), containing 100 mM NaCl and 1 mM $MgCl_2$, are shown in Figure 7. Under these solution conditions, equilibrium studies showed that the enzyme binding to the dsDNA is characterized by a large ω value of 35 ± 7 (*21*). A two-exponential fit provides an adequate description of the observed kinetics in the entire examined enzyme concentration range. Thus, the presence of positive cooperative interactions does not affect the number of observed normal modes of the reaction. As is evident from the trace corresponding to the nucleic acid alone (zero line), obtained at the same DNA concentration used with the protein but mixed with only the buffer, the two-exponential fit does not account for the total amplitude of the reaction, A_{Tot}. The data indicate that there is at least one additional fast step preceding the observed kinetic processes, with a relaxation time(s), too short to be extracted in the stopped-flow experiment.

The two resolved reciprocal relaxation times, $1/\tau_{S2}$ and $1/\tau_{S3}$, obtained from the experimental traces, as a function of the total rat pol β concentration, are shown in Figure 8a.

The values of $1/\tau_{S2}$ show a significant dependence upon polymerase concentration, approaching the plateau at high enzyme concentrations, while the values of $1/\tau_{S3}$ show little dependence upon enzyme concentration. Such behavior indicates that both relaxation times characterize intramolecular transitions of the formed complexes (*39*−*42*). Notice that τ_{S3} can be detected over the entire examined range of polymerase concentrations. The analysis of the observed kinetics has been performed using the same strategy described above for the negative cooperative case (Figure 6). There are four independent parameters, k_2, k_{-2}, ω_1, and ω_{-1}, that have to be determined. Simultaneous fitting of both individual relaxation times, $1/\tau_{S2}$ and $1/\tau_{S3}$, provides the initial values of K_1, k_2, k_{-2}, ω_1, and ω_{-1}. The computer simulations of the reciprocal relaxation times, $1/\tau_5-1/\tau_7$, using estimated equilibrium and rate parameters, are shown in Figure 8b. Relaxation time τ_7 is significantly longer than τ_5 and τ_6, indicating that the experimentally obtained τ_{S3} corresponds directly to τ_7, the slowest normal mode of the reaction. However, the values of relaxation times τ_5 and τ_6 differ by a factor of only ~2, making them practically indistinguishable in the fitting process, particularly if the amplitudes are of the same sign or if one amplitude dominates the observed kinetic process (see below) (*39*). In other words, what is observed in the experiment as τ_{S2} is, in fact, an average of two relaxation processes characterized by relaxation times τ_5 and τ_6, which are very close in value. This result indicates that rate parameters k_2 and k_{-2} and cooperativity factors ω_1 and ω_{-1} can only be approximated, with the approximation being better if the the difference between τ_5 and τ_6 is smaller and the contribution of the amplitude A_6 to the observed signal is smaller.

The collective amplitude of all fast normal modes, A_F, can be obtained from the known amplitudes of the observed processes, A_{S2} and A_{S3}, and the total amplitude of the reaction using eq 11. However, in the case of strong cooperative interactions, A_{S2} is also the collective amplitude defined as

$$A_{S2} = A_5 + A_6 \tag{13}$$

Thus

$$A_F = A_{Tot} - A_5 - A_6 - A_{S3} \tag{14}$$

The dependence of the normalized amplitudes, A_F, A_{S2}, and A_{S3}, upon the rat pol β concentration is shown in Figure 8c. The behavior is complex. At a low enzyme concentration, the collective amplitude of the fast processes, A_F, has negative values. As the concentration of the polymerase increases, A_F becomes positive. Values of the A_{S2} amplitude dominate the kinetic process at lower polymerase concentrations and decrease at higher enzyme concentrations. However, contrary to the low-cooperativity case, amplitude A_{S3} has significant and clearly detectable values over the entire examined enzyme concentration range. Because the values of $1/\tau_{S3}$ are very low as compared to $1/\tau_5$ and $1/\tau_6$, the slowest normal mode is effectively decoupled and $A_{S3} = A_7$.

Amplitude analysis has been performed using the approach analogous to the one described above for the negative cooperativity case, using equilibrium data (*21*). Therefore, fitting of the amplitudes begins by assigning the initial values of the molar fluorescence intensities to the complexes as follows: $F_1 = 1$, $F_2 = 2.2$, $F_3 = 2.2$, $F_4 = 2.2$, $F_5 = 2.2$, F_6

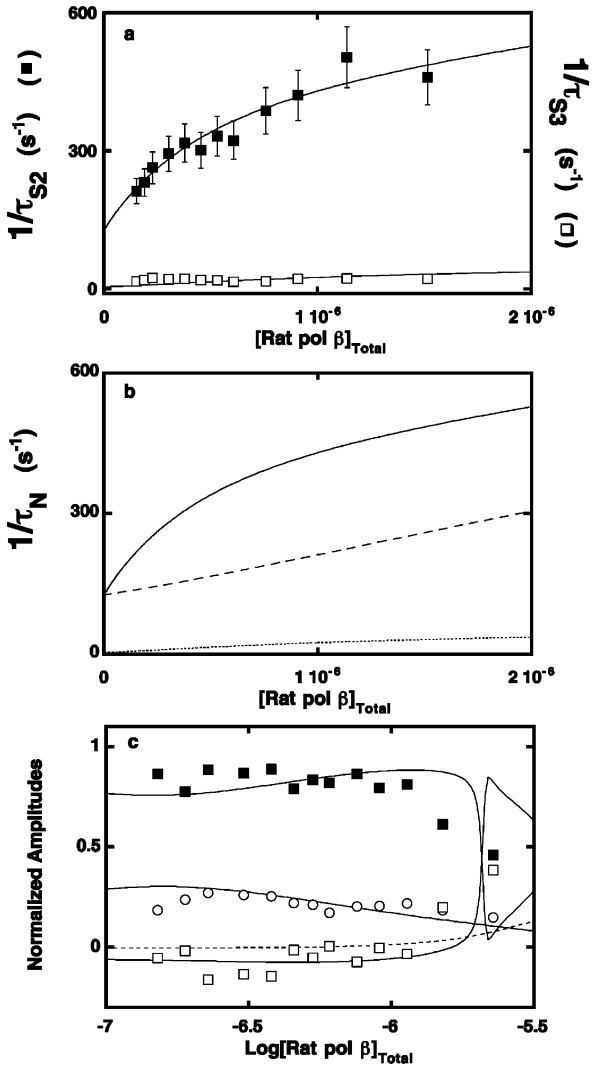

FIGURE 8: (a) Dependence of the reciprocal relaxation times, $1/\tau_{S2}$ (■) and $1/\tau_{S3}$ (□), for the binding of rat pol β to the dsDNA 10-mer, in buffer C (pH 7.0, 10 °C), containing 100 mM NaCl and 1 mM $MgCl_2$, upon the total concentration of the enzyme. The solid lines are nonlinear least-squares fits according to the mechanism, defined by Scheme 1, with a partial equilibrium association constant K_1 of 4.1×10^5 M^{-1} and the following rate constants and cooperativity factors: $k_2 = 375$ s^{-1} and $k_{-2} = 150$ s^{-1} and $\omega_1 = 0.15$ and $\omega_{-1} = 0.004$ (details in the text). The error bars are standard deviations obtained from three to four independent experiments. (b) Computer simulation of the reciprocal relaxation times, $1/\tau_5$ (—), $1/\tau_6$ (− − −), and $1/\tau_7$ (···), corresponding to slow normal modes of the reaction defined by Scheme 1, using kinetic parameters obtained in the fit of experimental relaxation times, $1/\tau_{S2}$ and $1/\tau_{S3}$ (details in the text). (c) Dependence of experimental relaxation amplitudes, for the binding of rat pol β to the dsDNA 10-mer in buffer C (pH 7.0, 10 °C), containing 100 mM NaCl and 1 mM $MgCl_2$, upon the total concentration of the enzyme. The solid lines are nonlinear least-squares fits according to the cooperative binding mechanism, defined by Scheme 1, with the following relative fluorescence intensities: $F_2 = 0.8$, $F_3 = 3.1$, $F_4 = 1.1$, $F_5 = 2.7$, $F_6 = 2.7$, $F_7 = 2.5$, and $F_8 = 2.3$. The maximum fluorescence increase of the nucleic acid is taken from the equilibrium fluorescence titration under the same solution conditions as the ΔF_{max} of 1.45 ± 0.1 (details in the text) (*21*). The rate constants are the same as in Figure 7a. The collective amplitude that includes four fast normal modes of the reaction $A_F = A_1 + A_2 + A_3 + A_4$ (□). The collective amplitude $A_{S2} = A_5 + A_6$ (■) or A_7 (○). The dashed line is the theoretical dependence of amplitude A_6 upon the rat pol β concentration, obtained for the determined rate and spectroscopic parameters (Table 2).

$= 2.5$, $F_7 = 2.5$, and $F_8 = 2.5$ (*21*). In the final step of the analysis, global fitting that simultaneously includes relaxation times and amplitudes refines the values of the rate constants and molar fluorescence parameters. The solid lines in panels a and c of Figure 8 are computer fits of the relaxation times and amplitudes, according to the mechanism depicted in Scheme 1, using a single set of spectroscopic and rate parameters. Contrary to the data obtained in the absence of magnesium, the molar fluorescence intensities characterizing N_2 and N_4 intermediates are significantly lower than observed in the absence of Mg^{2+} (Tables 1 and 2), indicating that magnesium affects the structure of these intermediates (see the Discussion). We also included the computer simulation of amplitude A_6 in Figure 8c. Its values contribute to the observed collective amplitude A_{S2} at only high enzyme concentrations. The obtained rate and fluorescence parameters are included in Table 2.

Effect of Salt on the Dynamics of the Cooperative Binding of Rat Pol β to the dsDNA in the Absence and Presence of Magnesium Cations. The stopped-flow kinetic experiments with the binding of rat pol β to the dsDNA as a function of salt concentration in the absence of magnesium cations have been performed in an analogous way as described above. The obtained rate constants, partial equilibrium constants, and spectroscopic parameters are included in Table 1. As can be seen, the increased salt concentration in solution does not affect the mechanism of the reaction; however, it does affect the dynamics of the partial steps. The forward and backward rate constants of the conformational transition of the bound polymerase are differently affected by the increase in the salt concentration in solution. The value of k_2 is affected little by the salt, while k_{-2} increases at higher NaCl concentrations. As a result, at increased salt concentrations, the conformational transition becomes less energetically favorable. An opposite effect is observed in the case of the cooperative interactions. There is a clear increase in ω_1 and a significant decrease in ω_{-1}, resulting in a strong increase in the cooperativity parameter ω at elevated NaCl concentrations (Table 1).

The dependence of the logarithm of the intrinsic binding constant, K_{int}, upon the logarithm of the NaCl concentration is shown in Figure 9a (log−log plot) (*46*, *47*). The plot is linear in the examined salt concentration range and characterized by the slope $\partial(\log K_{int})/\partial(\log[NaCl])$ of -3.6 ± 0.5, indicating that the release of ~3.6 ions accompanies the intrinsic binding of the enzyme to the nucleic acid. The analogous $\partial(\log K_{int})/\partial(\log[NaCl])$ value of -4.0 ± 0.5 has been previously obtained for the same system in equilibrium studies (*21*). The dependence of the logarithm of the equilibrium constant, K_1, characterizing the bimolecular step, upon the logarithm of NaCl concentration (log−log plot), is included in Figure 9a. The slope of the linear plot, $\partial(\log K_1)/\partial(\log[NaCl])$, is -2.4 ± 0.4, indicating that the net release of ~2.4 ions occurs in the bimolecular step. Nevertheless, the salt dependence of K_1 cannot account for the observed total net ~3.6 ions released upon the enzyme binding to the dsDNA. A log−log plot for the equilibrium constant, K_2, describing the conformational transition of the bound polymerase molecule, is also included in Figure 9a. The plot is characterized by the slope $\partial(\log K_2)/\partial(\log[NaCl])$ of -1.7 ± 0.3 indicating a net release of ~1.7 ions that accompanies the conformational transition of the bound

Table 2: Kinetic, Thermodynamic, and Spectroscopic Parameters Characterizing the Cooperative Binding of Rat Pol β to the dsDNA 10-mer, in Buffer C (pH 7, 10 °C), Containing 1 mM $MgCl_2$ and Different NaCl Concentrations

[NaCl] (mM)	K_1 (M^{-1})	k_2 (s^{-1})	k_{-2} (s^{-1})	ω_1	ω_{-1}	K_2	ω	K_{int} (M^{-1})	F_2[a]	F_3[a]	F_4[a]	F_5[a]	F_6[a]	F_7[a]	F_8[a]
50	$(2.3 \pm 0.7) \times 10^6$	750 ± 55	60 ± 15	0.14 ± 0.005	0.1 ± 0.01	12.5 ± 3.6	1.4 ± 0.4	$(3.2 \pm 1) \times 10^7$	0.8 ± 0.1	3.0 ± 0.1	1.4 ± 0.1	2.4 ± 0.1	2.2 ± 0.1	2.2 ± 0.1	2.5 ± 0.1
75	$(6.9 \pm 2) \times 10^5$	490 ± 40	100 ± 18	0.06 ± 0.005	0.006 ± 0.001	4.9 ± 1.3	10 ± 3.5	$(4.1 \pm 1.5) \times 10^6$	1.5 ± 0.05	3.0 ± 0.1	1.5 ± 0.1	2.5 ± 0.1	2.2 ± 0.1	2.2 ± 0.1	2.6 ± 0.1
100	$(4.1 \pm 1.3) \times 10^5$	375 ± 40	150 ± 20	0.15 ± 0.01	0.004 ± 0.001	2.5 ± 0.8	37.5 ± 11	$(1.4 \pm 0.5) \times 10^6$	0.8 ± 0.1	3.1 ± 0.1	1.1 ± 0.1	2.7 ± 0.1	2.7 ± 0.1	2.5 ± 0.1	2.3 ± 0.1
125	$(1.8 \pm 0.6) \times 10^5$	370 ± 35	200 ± 35	0.12 ± 0.01	0.0016 ± 0.0003	1.9 ± 0.5	75 ± 21.7	$(5.1 \pm 1.5) \times 10^5$	0.7 ± 0.1	5.3 ± 0.1	1.0 ± 0.1	2.5 ± 0.1	2.5 ± 0.1	2.8 ± 0.1	2.2 ± 0.1

[a] Values relative to the fluorescence ($F_1 = 1$) of the free dsDNA 10-mer (details in the text).

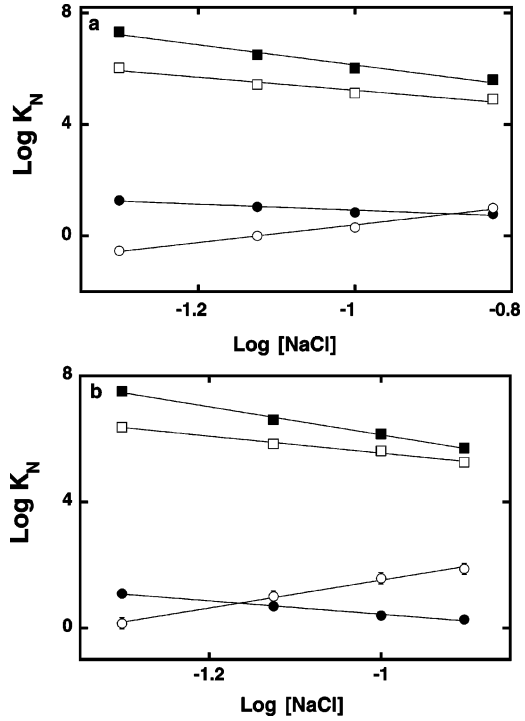

FIGURE 9: (a) Dependence of the logarithm of the intrinsic equilibrium binding constant, K_{int} (■), the partial equilibrium constant, K_1, characterizing the bimolecular step (□), the partial equilibrium constant, K_2, characterizing the conformational transition of the bound polymerase to the dsDNA (●), and the cooperative interaction parameter, ω (○), upon log[NaCl] (log−log plots) in buffer C (pH 7.0, 10 °C). The plots are characterized by the following slopes: $\partial(\log K_{int})/\partial(\log[NaCl]) = -3.6 \pm 0.5$, $\partial(\log K_1)/\partial(\log[NaCl]) = -2.4 \pm 0.4$, $\partial(\log K_2/\partial(\log[NaCl]) = -1.7 \pm 0.3$, and $\partial(\log \omega)/\partial(\log[NaCl]) = 3.2 \pm 0.5$. (b) Dependence of the logarithm of the intrinsic equilibrium binding constant, K_{int} (■), the partial equilibrium constant, K_1, characterizing the bimolecular step (□), the partial equilibrium constant, K_2, characterizing the conformational transition of the bound polymerase to the dsDNA (●), and the cooperativity interaction parameter, ω (○), upon log-[NaCl] in buffer C (pH 7.0, 10 °C) containing 100 mM NaCl and 1 mM $MgCl_2$. The plots are characterized by the following slopes: $\partial(\log K_{int})/\partial(\log[NaCl]) = -4.4 \pm 0.5$, $\partial(\log K_1)/\partial(\log[NaCl]) = -2.7 \pm 0.4$, $\partial(\log K_2)/\partial(\log[NaCl]) = -2.1 \pm 0.4$, and $\partial(\log \omega)/\partial(\log[NaCl]) = 4.4 \pm 0.5$.

enzyme molecule. Thus, the total ion release accompanying the intrinsic binding of rat pol β to the dsDNA occurs in both the initial binding step and the conformational transition of the bound enzyme.

The dependence of the cooperativity parameter ω upon the salt concentration is shown in Figure 9a. Contrary to the partial equilibrium constants characterizing the intrinsic binding, the linear log−log plot is characterized by a positive slope [$\partial(\log \omega)/\partial(\log[NaCl]) = 3.2 \pm 0.5$] indicating that a net uptake of $\sim$ 3.2 ions accompanies the engagement of the enzyme in cooperative interactions. The obtained net uptake of ions is, within experimental accuracy, identical to the value of the corresponding parameter determined in equilibrium studies (*21*) (see the Discussion).

The rate constants, partial equilibrium constants, and spectroscopic parameters obtained at different salt concentrations, in the presence of 1 mM $MgCl_2$, are included in Table 2. The response of the partial equilibrium steps of the cooperative binding of pol β to the dsDNA to the increased salt concentration, in the presence of magnesium, is more pronounced than that observed in the absence of Mg^{2+}. The dependence of the logarithm of the intrinsic binding constant, K_{int}, upon the logarithm of the NaCl concentration is shown in Figure 9b. The slope of the plot, $\partial(\log K_{int})/\partial(\log[NaCl])$, equals -4.4 ± 0.5, which indicates that the total net release of $\sim$4.4 ions accompanies the intrinsic step. This value is in good agreement with the analogous parameter (-5.1 ± 0.5) obtained in equilibrium titrations (*21*). The log−log plot of the partial equilibrium constant, K_1, for the bimolecular step is characterized by a slope $\partial(\log K_1)/\partial(\log[NaCl])$ of -2.7 ± 0.4 which indicates that the release of $\sim$2.7 ions accompanies the bimolecular step. Thus, the net release of ions in the bimolecular step is slightly larger than that observed in the absence of magnesium (Figure 9a). The log−log plot of the partial equilibrium constant, K_2, describing the conformational transition of the bound polymerase, is characterized by a slope $\partial(\log K_2)/\partial(\log[NaCl])$ of -2.1 ± 0.4 and is also slightly larger than the $\partial(\log K_2)/\partial(\log[NaCl])$ value of -1.7 ± 0.3 observed in the absence of Mg^{2+}. Moreover, the slope of the log−log plot of the cooperativity parameter, ω, $\partial(\log \omega)/\partial(\log[NaCl])$, of 4.4 ± 0.5 is larger than the value of 3.2 ± 0.5 observed in the absence of magnesium and very close to the value of 4.5 ± 0.5 determined in equilibrium studies (*21*).

DISCUSSION

Stopped-Flow Kinetics of Cooperative Ligand Binding to a One-Dimensional Lattice. Thermodynamics and kinetics of cooperative binding of a large ligand to a one-dimensional lattice have been the subject of intensive research (*48*−*55*). The interest in this basic problem stems from the fact that many functional protein−nucleic acid interactions include binding of a large protein molecule to long stretches of nucleic acid lattices (*48*−*54*). Sophisticated kinetic studies of such protein−nucleic acid systems focus so far, predominantly, on analyses of the bimolecular step of the reaction (*48*−*54*). However, complete kinetic analyses of the protein−nucleic acid binding requires examination of possible conformational changes of the bound protein as well as the dynamics of cooperative interactions between bound protein molecules.

There are two characteristic features of large ligand−one-dimensional lattice interactions. First, a large ligand covers more than one residue of the lattice; i.e., the stoichiometry of the ligand−lattice system is defined by the site size of the complex, *p*, which is the number of lattice monomers occluded by the ligand. Thus, at saturation, the number of bound ligand molecules is equal to the total number of lattice monomers divided by the site size of the complex. Second, instead of discrete binding sites, the interacting system has potential binding sites whose number changes in a nonlinear fashion as a function of the degree of binding (*34*−*38*). In this context, complete kinetic analyses of the cooperative large ligand binding to a long polymer lattice would be prohibitively difficult. On the other hand, the smallest possible system that preserves all necessary ingredients of cooperative binding includes a lattice that, at saturation, can accept only two ligand molecules, i.e., a two-binding site lattice (*55*). This simplest binding model is depicted in Figure 1 and its kinetic mechanism in Scheme 1. Although it is still a very complex mechanism, it allows the experimenter to address most of the major features of the system, including

cooperativity and intramolecular conformational transitions of the formed complexes.

An assumption in the model depicted in Scheme 1 is that the bimolecular step is close to the diffusion-controlled limit. One can test this assumption by examining the resolution of the first step as a function of the ligand concentration. Another assumption is that changes in the location of the bound ligand on the lattice occur through the dissociation from the lattice, not through a possible translocation along the lattice (*48*−*55*). This is a very reasonable assumption, if justified by the data. Thus, a very large k_1 and, in particular, the dissociation constant, k_{-1}, strongly suggest that the ligand leaves the lattice before any translocation, if it occurs, along the lattice can take place. The data for the kinetics of binding of pol β to the ssDNA and very fast binding step observed for the dsDNA indicate that the association rate constants are very close to the diffusion-controlled ones; thus, for the partial equilibrium constant $K_1 \times 10^6$ M^{-1}, the dissociation constant, k_{-1}, must be in the range of $\sim 1 \times 10^3$ to 1×10^4 s^{-1} (Table 1) (*18*, *19*). A simplification introduced into the model is that cooperative interactions are averaged over different conformational states of the bound enzyme. However, this simplification can be tested by comparison between the cooperativity parameters obtained from kinetic data with the same parameters obtained directly from equilibrium studies (see below). There are seven normal modes in the model depicted in Scheme 1. Extracting all relaxation times for the mechanism, in practice, is not possible (Figures 6a and 8a). The analysis presented here provides general guidelines for examination of the kinetics of such complex cooperative interactions. An absolutely necessary condition for this approach is the quantitative analysis of equilibrium properties of the binding process (*18*, *19*, *40*−*42*).

Intrinsic Binding of Rat Pol β to the dsDNA Includes Two Sequential Steps. Studies described in this work provide, for the first time, direct insight into the dynamics and energetics of interactions of rat pol β with the dsDNA. The intrinsic binding of the enzyme to the dsDNA includes two steps: very fast bimolecular association followed by a conformational transition. Although the bimolecular step provides the major contribution to the free energy of binding, the second step is also energetically favorable, particularly at low salt concentrations and in the absence of magnesium (Tables 1 and 2). The same number of observed relaxation times in the presence of the excess of the protein or the nucleic acid strongly indicates that the enzyme does not exist in a pre-equilibrium conformational transition prior to the dsDNA binding (*18*, *19*, *39*−*42*). The multistep sequential mechanism of enzyme binding has been found also for interactions with the ssDNA, in its (pol β)$_5$ and (pol β)$_{16}$ binding modes, and gapped DNA substrates, indicating the lack of the pre-equilibrium conformational transition of the enzyme (*18*−*20*). However, this result need not be automatically applicable to interactions with the dsDNA. Different DNA conformations may probe different sets of conformational states of the enzyme. The sequential mechanism indicates that the dsDNA does not select between different states of the polymerase (see above).

Mechanism of Intrinsic Binding of Rat Pol β to the dsDNA Is Different from the Mechanism of Binding to the ssDNA. Different Orientations of the Enzyme in Complexes with the ss- and dsDNA. Although the mechanism of the binding of the polymerase to the ssDNA and the mechanism of the intrinsic binding to the dsDNA are both sequential and initiated by a fast bimolecular step, the similarity between the binding mechanisms ends there. Interactions with the ssDNA are characterized by a mechanism that includes at least three steps, instead of only two steps observed for the dsDNA. There are significant differences between transitions following the bimolecular step, indicating a different nature of both transitions. The rate constant k_2 (838 ± 65 s^{-1}) is significantly larger and the backward rate constant k_{-2} (44 ± 12 s^{-1}) much lower for the binding to the dsDNA as compared to the corresponding parameters ($k_2 = 144 \pm 30$ s^{-1} and $k_{-2} = 300 \pm 50$ s^{-1}) for the binding to the ssDNA under the same solution conditions (*18*). As a result, in the case of the ssDNA, the conformational transition following the bimolecular step is energetically unfavorable with the partial equilibrium constant [$K_2 = 0.48 \pm 0.16$ (50 mM NaCl)]. The value of the equilibrium constant K_2 is 18.9 ± 9 for the dsDNA; i.e., it is by a factor of $\sim$40 higher than that observed for the pol β−ssDNA system (Table 1).

Such different behavior occurs, although the enzyme associates with the DNA, using always its 8-kDa domain, in a manner that is independent of the conformation of the nucleic acid (*12*, *18*, *19*, *21*). As we pointed out before, there are clear differences between the binding of the isolated 8-kDa domain to the ss- and dsDNA, and between the isolated domain and the intact enzyme (*8*−*12*). Interactions of the isolated 8-kDa domain with the ssDNA are characterized by very weak cooperative interactions with an ω of 1.4−4. However, the domain binds with strong positive cooperative interactions to the dsDNA with an ω of 90 ± 30 (*12*). The site size of the intact enzyme in its (pol β)$_5$ binding mode, where only the 8-kDa domain is engaged in interactions with the nucleic acid, is 5 ± 2 nucleotides. On the other hand, in the complexes of the isolated domain with the ss- and dsDNA, the site size is 9 ± 0.6 nucleotide residues and 9 ± 2 bp, respectively (*12*). These data were the first indication that the 8-kDa domain is capable of binding the ss- and dsDNA in different orientations, resulting in different site sizes and cooperative interactions.

Kinetic data indicate that multiple conformational transitions following the bimolecular step, in complexes with the ssDNA, in the (pol β)$_{16}$ and (pol β)$_5$ binding mode, are generated at the interfaces of the 8-kDa domain and the nucleic acid (*18*, *19*). Because the enzyme does not engage its 31-kDa domain in interactions either with dsDNA or with the ssDNA in the (pol β)$_5$ binding mode, the large difference in the nature of the transition following the bimolecular step, in the complex with the dsDNA as compared to the ssDNA, strongly suggests that the enzyme forms different complexes, even in the first binding step, with both conformations of the nucleic acid (*18*, *19*, *21*). In other words, kinetic data described in this work strongly support the conclusion that the orientations of the bound pol β molecule in the complexes with the ss- and dsDNA are different and imposed at the interface of the 8-kDa domain−nucleic acid complex.

The Transition following the Bimolecular Step Does Not Facilitate the Engagement of the Enzyme in Cooperative Interactions. At low salt concentrations (50 mM NaCl), the conformational transition following the bimolecular complex is energetically most favorable and characterized by values for partial equilibrium constant K_2 of 18.9 ± 9 and $12.5 \pm$

3.6 in the absence and presence of magnesium cations, respectively. At the same salt concentrations, cooperative interactions are negative, with an ω of 0.29 ± 0.14, or weakly positive, with an ω of 1.4 ± 0.4 (Tables 1 and 2). Analogous parameters obtained in equilibrium studies, under the same solution conditions, are 0.31 ± 0.06 and 1 ± 0.5, respectively (*21*). Notice that the increasing salt concentration decreases the partial equilibrium constant K_2, making the transition less energetically favorable. The same NaCl concentration increase leads to significantly stronger positive cooperative interactions, particularly in the presence of magnesium (Tables 1 and 2). Such behavior of the system indicates that the conformational transition following the bimolecular step is not involved in the formation of cooperative interactions between bound protein molecules. The excellent agreement between the values of ω obtained from equilibrium and kinetic measurements strongly corroborates this conclusion. Rather, the role of the transition seems to be reinforcing the moderate affinity for the dsDNA, resulting from the bimolecular step.

Salt and Magnesium Affect both Bimolecular and Conformational Transitions of the Intrinsic Binding of the Pol β−dsDNA Complex. In the absence of magnesium, the total net number of ions released in the intrinsic binding process equals $\partial(\log K_{int})/\partial(\log[NaCl])$ (-3.6 ± 0.5), indicating that the release of ~3.6 ions accompanies the intrinsic binding of the enzyme to the dsDNA (Figure 9a). The analogous value obtained from equilibrium studies is -4.0 ± 0.5. As pointed out above, such good agreement between the kinetic and equilibrium results provides additional evidence of the correctness of the kinetic analysis. Kinetic data indicate that the net ion release is generated in the bimolecular step and also in the conformational transition following the binding with corresponding slopes: $\partial(\log K_1)/\partial(\log[NaCl]) = -2.4 \pm 0.4$ and $\partial(\log K_2)/\partial(\log[NaCl]) = -1.7 \pm 0.3$, respectively (Figure 9a). It is evident that the bimolecular step does not dominate the release of the ion from the complex. A similar salt effect that includes both a bimolecular step and a following conformational transition has been observed in the polymerase−ssDNA association (*18*, *19*). These data point out an important caveat in interpreting the salt effect exclusively in terms of a single step of the protein binding to the nucleic acid.

In the presence of magnesium, $\partial(\log K_{int})/\partial(\log[NaCl]) = -4.4 \pm 0.5$; thus, the total net number of ions released is increased. The observed increase originates from both the bimolecular step, with a $\partial(\log K_1)/\partial(\log[NaCl])$ value of -2.7 ± 0.4, and the following conformational transition [$\partial(\log K_2)/\partial(\log[NaCl]) = -2.1 \pm 0.4$]. The analogous increase in the total net number of ions released in the presence of magnesium was observed previously in equilibrium studies (*21*). The magnesium effect is surprising. A rather strong decrease in the net number of ions released is always expected, particularly for the bimolecular step, due to the competition between Mg^{2+} and Na^+ for the DNA (*46*, *47*). Recall that pol β associates with the dsDNA using only its 8-kDa domain (*21*). The specific effect of magnesium on interactions of the isolated 8-kDa domain with the ssDNA has been described by us previously (*12*). The effect includes changes in the site size of the 8-kDa domain complex with the ssDNA and the number of anions released from the domain accompanying association with the nucleic acid. The presence of magnesium also affects the anions released in the intact enzyme−dsDNA interactions (*21*). Magnesium binding sites participating in the process are characterized by a binding constant of $\geq 10^4$ M^{-1}, indicating that, under the solution conditions that were examined, the Mg^{2+} effect results from the binding of magnesium cations to the domain and/or the enzyme, and not to the ssDNA (*12*). As mentioned above, particularly surprising is the fact that the presence of magnesium does not decrease but even slightly increases the number of ion released in the first bimolecular complex. Amplitude analysis shows that there is a significant increase in the nucleic acid fluorescence induced already in the bimolecular step, indicating that, despite its very fast nature, it is not a simple encounter complex (*18*, *19*, *56*). In the presence of Mg^{2+}, this fluorescence increase is strongly diminished (Tables 1 and 2). Thus, the data indicate that specific Mg^{2+} cations binding to the polymerase induce a different conformational state of the enzyme that has a different thermodynamic response in interactions with the DNA, including the bimolecular step.

As mentioned above, kinetic data indicate that two partial binding steps share the salt effect on the intrinsic binding of the polymerase to the dsDNA. Such sharing may have important functional and mechanistic implications. It strongly decreases the sensitivity of the bimolecular step to the increased salt concentration, allowing the polymerase to preserve to a large extent its initial binding affinity for the nucleic acid, residing in the bimolecular step at elevated salt concentrations. On the other hand, binding to the dsDNA is an initial stage in the enzyme search for the ssDNA gap in the damaged DNA (*1*−*6*). A decreased affinity and slowing of the second step would facilitate the detachment of the polymerase from the ds conformation, once the gapped DNA is encountered (see below).

Mechanism of the Binding of Rat Pol β to the dsDNA Is Not Affected by the Changing Character of Cooperative Interactions between Bound Enzyme Molecules as a Function of Salt and Magnesium Concentration. Cooperative interactions between bound pol β molecules exhibit behavior very different from the intrinsic binding to the dsDNA (*21*). Thus, instead of a release, an uptake of ions accompanies the engagement in cooperative interactions (Figure 9a,b). It is interesting that despite the dramatic change in the nature of cooperative interactions, as a function of salt and magnesium concentration, the general feature of the kinetic mechanism, i.e., the number of relaxation steps, is unaffected. As discussed above, the conformational transition in the intrinsic binding event is not coupled to the cooperative interactions, indicating that the orientation of the enzyme that favors the engagement in cooperative contacts has already been reached in the bimolecular step. Moreover, equilibrium data indicate that a significant net uptake of anions occurs in the formation of cooperative contacts (*21*). Because the negatively charged DNA does not bind anions, the large contribution of anions to the net ion uptake provides evidence that cooperative interactions result from direct protein−protein interactions. The independence of the mechanism of enzyme binding with respect to the nature of cooperative interactions strongly suggests that protein surfaces that engage in cooperative contacts are already in the proper orientation after the bimolecular step, and simply need binding of ions, including anions, to provide a bridge for efficient contacts. Notice that

amplitude analysis indicates only moderate changes in fluorescence intensities of protein−dsDNA complexes, as a result of engagement in cooperative interactions (Tables 1 and 2). This observation indicates that the interface of the protein−DNA complex is affected little by cooperative interactions.

Functional Implications of the Dynamics of Cooperative Binding of Rat Pol β to the dsDNA. Kinetic and thermodynamic studies indicate that rat pol β preferentially binds to the dsDNA conformation over the ssDNA, mostly due to the amplifying effect of cooperative interactions between bound enzyme molecules. This behavior excludes the possibility that the intrinsic affinity of the enzyme for the ssDNA alone plays any significant role in the recognition of the gapped DNA by the polymerase (*8*−*12*). Although the intrinsic affinity of the gap complex is significantly higher than the intrinsic affinity for the dsDNA, this is only because both DNA-binding subsites of the polymerase engage in interactions with the DNA in the gap complex (*10*). Recently, we have proposed a plausible model of the possible role of cooperative binding to the dsDNA in recognition of a damaged gapped DNA (*21*). The enzyme cooperatively binds to the dsDNA, using exclusively the 8-kDa domain and with the site size (*p*) of 5 bp. Cooperative interactions prevent the enzyme from dissociating. A protein cluster is formed that allows the enzyme to examine longer patches of the dsDNA until the damaged DNA, the ssDNA gap, is encountered. Cooperative interactions with pol β in the cluster bound to the dsDNA become weak, as observed experimentally (*21*). In other words, the enzyme, encountering the gap, breaks its ties with the protein cluster and forms a gap complex. The enzyme can now engage the 31-kDa domain in interactions with the DNA and initiate catalytic steps.

Kinetic analyses described in this work provide mechanistic information about the events at the moment the gapped DNA is encountered. The affinity of the enzyme for the dsDNA is reinforced not only by cooperative interactions but also by a conformational transition following the bimolecular step. The transition is fast with a forward rate constant k_2 of ∼750−370 s^{-1}, and energetically favorable (Table 2). The engagement in cooperative interactions is much slower and characterized by an association cooperativity factor ω_1 of ∼0.15−0.06. However, a docking step of the enzyme on the ssDNA gap is even more energetically favorable than the conformational transition in the intrinsic binding to the dsDNA, particularly in the presence of magnesium, and very fast with a forward rate constant k_2 of 1100−430 s^{-1} (*20*, *57*). In other words, at the moment the gap is encountered, the rate of engagement in the gap complex is by a factor of ∼11 faster than the engagement in cooperative interactions with pol β molecules bound to the dsDNA. If the polymerase molecule is already in the cluster on the dsDNA, it will efficiently transform into the gap complex, due to a much higher affinity of the gap complex, albeit with the rate affected by the rate of release from cooperative interactions, thus breaking its ties with the cluster. However, any incoming enzyme molecule will not engage in the cooperative interaction with the cluster on the dsDNA because of the large difference between the rates of the cooperative binding and the formation of the gap complex. The enzyme will directly form the gap complex.

ACKNOWLEDGMENT

We thank Dr. Aaron Lucius for reading and commenting on the manuscript.

SUPPORTING INFORMATION AVAILABLE

UV melting curve of the dsDNA 10-mer substrate. This material is available free of charge via the Internet at http://pubs.acs.org.

REFERENCES

1. Friedberg, E. C., Walker, G. C., and Siede, W. (1995) in *DNA Repair and Mutagenesis*, pp 317−365, ASM Press, Washington, DC.
2. Kornberg, A., and Baker, T. A. (1992) in *DNA Replication*, pp 197−225, W. H. Freeman, New York.
3. Budd, M. E., and Campbell, J. L. (1997) The roles of the eucaryotic DNA polymerases in DNA repair synthesis, *Mutat. Res. 384*, 157−167.
4. Fry, M., and Loeb, L. A. (1986) in *Animal Cell DNA Polymerases*, pp 75−183, CRC Press, Boca Raton, FL.
5. Hubscher, U., Nasheuer, H.-P., and Syvaoja, J. E. (2000) Eukaryotic DNA polymerases, a growing family, *Trends Biochem. Sci. 25*, 143−147.
6. Masumoto, Y., and Kim, K. (1995) Excision of deoxyribose phosphate residues by DNA polymerase β during DNA repair, *Science 269*, 699−702.
7. Pelletier, H., Sawaya, M. R., Wolfle, W., Wilson, S. H., and Kraut, J. (1996) A structural basis for metal ion mutagenicity and nucleotide selectivity in human DNA polymerase β, *Biochemistry 35*, 12762−12777.
8. Rajendran, S., Jezewska, M. J., and Bujalowski, W. (1998) Human DNA polymerase β recognizes single-stranded DNA using two different binding modes, *J. Biol. Chem. 273*, 31021−31031.
9. Jezewska, M. J., Rajendran, S., and Bujalowski, W. (1998) Transition between different binding modes in rat DNA polymerase β−ssDNA complexes, *J. Mol. Biol. 284*, 1113−1131.
10. Rajendran, S., Jezewska, M. J., and Bujalowski, W. (2001) Recognition of template primer and gapped DNA substrates by human DNA polymerase β, *J. Mol. Biol. 308*, 477−500.
11. Jezewska, M. J., Rajendran, S., and Bujalowski, W. (2001) Energetics and specificity of rat DNA polymerase β interactions with template-primer and gapped DNA substrates, *J. Biol. Chem. 276*, 16123−16136.
12. Jezewska, M. J., Rajendran, S., and Bujalowski, W. (2001) Interactions of the 8-kDa Domain of Rat DNA Polymerase β with DNA, *Biochemistry 40*, 3295−3307.
13. Matsumoto, Y., Kim, K., Katz, D. S., and Feng, J. A. (1998) Catalytic center of DNA polymerase β for excision of deoxyribose phosphate groups, *Biochemistry 37*, 6456−6464.
14. Nagasawa, K., Kitamura, K., Yasui, A., Nimura, Y., Ikeda, K., Hirai, M., Matsukage, A., and Nakanishi, M. (2000) Identification and characterization of human DNA polymerase β2, a DNA polymerase β-related enzyme, *J. Biol. Chem. 275*, 31233−31238.
15. Dominguez, O., Ruiz, J. F., Lain de Lera, T., Garcia-Diaz, M., Gonzalez, M. A., Kirchhoff, T., Martinez, A. C., Bernad, A., and Blanco, L. (2000) DNA polymerase mu (Pol μ), homologous to TdT, could act as a DNA mutator in eukaryotic cells, *EMBO J. 19*, 1731−1742.
16. Garcia-Diaz, M., Dominguez, O., Lopez-Fernandez, L. A., de Lera, L. T., Saniger, M. L., Ruiz, J. F., Parraga, M., Garcia-Ortiz, M. J., Kirchhoff, T., del Mazo, J., Bernad, A., and Blanco, L. (2000) DNA polymerase lambda (Pol λ), a novel eukaryotic DNA polymerase with a potential role in meiosis, *J. Mol. Biol. 301*, 851−867.
17. Oliveros, M., Yanez, R. J., Salas, M. L., Salas, J., Vinuela, E., and Blanco, L. (1997) Characterization of an African swine fever virus 20-kDa DNA polymerase involved in DNA repair, *J. Biol. Chem. 272*, 30899−30910.
18. Jezewska, M. J., Rajendran, S., Galletto, R., and Bujalowski, W. (2001) Kinetic Mechanisms of Rat Polymerase β−ssDNA Interactions. Quantitative Fluorescence Stopped-Flow Analysis of the Formation of the $(Pol\ \beta)_{16}$ and $(Pol\ \beta)_5$ Binding Mode, *J. Mol. Biol. 313*, 977−1002.

19. Rajendran, S., Jezewska, M. J., and Bujalowski, W. (2001) Multiple-step kinetic mechanisms of the ssDNA recognition process by human polymerase β in its different ssDNA binding modes, *Biochemistry 40*, 11794−11810.
20. Jezewska, M. J., Galletto, R., and Bujalowski, W. (2002) Dynamics of Gapped DNA Recognition by Human Polymerase β, *J. Biol. Chem. 277*, 20316−20327.
21. Jezewska, M. J., Galletto, R., and Bujalowski, W. (2003) Rat polymerase β binds double-stranded DNA using exclusively the 8-kDa domain. Stoichiometries, intrinsic affinities, and cooperativities, *Biochemistry 42*, 5955−5970.
22. Edeldoch, H. (1967) Spectroscopic determination of tryptophan and tyrosine in proteins, *Biochemistry 6*, 1948−1954.
23. Gill, S. C., and von Hippel, P. H. (1989) Calculation of protein extinction coefficients from amino acid sequence data, *Anal. Biochem. 182*, 319−326.
24. Jezewska, M. J., Rajendran, S., and Bujalowski, W. (1998) Complex of *Escherichia coli* Primary Replicative Helicase DnaB Protein with a Replication Fork. Recognition and Structure, *Biochemistry 37*, 3116−3136.
25. Jezewska, M. J., Rajendran, S., and Bujalowski, W. (1998) Functional and Structural Heterogeneity of the DNA Binding of the *E. coli* Primary Replicative Helicase DnaB Protein, *J. Biol. Chem. 273*, 9058−9069.
26. Jezewska, M. J., Rajendran, S., Bujalowska, D., and Bujalowski, W. (1998) Does ssDNA Pass Through the Inner Channel of the Protein Hexamer in the Complex with the *E. coli* DnaB Helicase? Fluorescence Energy Transfer Studies, *J. Biol. Chem. 273*, 10515−10529.
27. Azumi, T., and McGlynn, S. P. (1962) Polarisation of the Luminescence of Phenantrene, *J. Chem. Phys. 37*, 2413−2420.
28. Lakowicz, J. R. (1999) in *Principles of Fluorescence Spectroscopy*, pp 367−443, Plenum Press, New York.
29. Valeur, B. (2002) in *Molecular Fluorescence*, pp 155−199, Wiley-VCH, Weinheim, Germany.
30. Bujalowski, W., and Klonowska, M. M. (1993) Negative Cooperativity in the Binding of Nucleotides to *Escherichia coli* Replicative Helicase DnaB Protein. Interactions with Fluorescent Nucleotide Analogs, *Biochemistry 32*, 5888−5900.
31. Jezewska, M. J., and Bujalowski, W. (1996) A General Method of Analysis of Ligand Binding to Competing Macromolecules Using the Spectroscopic Signal Originating from a Reference Macromolecule. Application to *Escherichia coli* Replicative Helicase DnaB Protein−Nucleic Acid Interactions, *Biochemistry 35*, 2117−2128.
32. Bujalowski, W., and Jezewska, M. J. (1995) Interactions of *Escherichia coli* Primary Replicative Helicase DnaB Protein with Single-Stranded DNA. The Nucleic Acid Does Not Wrap Around the Protein Hexamer, *Biochemistry 34*, 8513−8519.
33. Bujalowski, W., and Jezewska, M. J. (2000) in *Spectrophotometry & Spectrofluorimetry. A Practical Approach* (Gore, M. G., Ed.) pp 141−165, Oxford University Press, Oxford, U.K.
34. Hill, T. L. (1985) *Cooperativity Theory in Biochemistry*, pp 25−61, Springer-Verlag, New York.
35. Lohman, T. M., and Bujalowski, W. (1991) Thermodynamic Methods for Model-Independent Determination of Equilibrium Binding Isotherms for Protein-DNA Interactions: Spectroscopic Approaches to Monitor Binding, *Methods Enzymol. 208*, 258−290.
36. Epstein, I. R. (1978) Cooperative and Non-cooperative Binding of Large Ligands to a Finite One-Dimensional Lattice. A Model For Ligand−Oligonucleotide Interactions, *Biophys. Chem. 8*, 327−339.
37. McGhee, J. D., and von Hippel, P. H. (1974) Theoretical aspects of DNA−protein interactions: Cooperative and noncooperative binding of large ligands to a one-dimensional homogeneous lattice, *J. Mol. Biol. 86*, 469−489.
38. Bujalowski, W., Lohman, T. M., and Anderson, C. F. (1989) On the Cooperative Binding of Large Ligand to a One-Dimensional Homogeneous Lattice: The Generalized Three-State Lattice Model, *Biopolymers 28*, 1637−1643.
39. Bernasconi, C. J. (1976) *Relaxation Kinetics*, pp 98−129, Academic Press, New York.
40. Bujalowski, W., and Jezewska, M. J. (2000) Kinetic mechanism of the single-stranded DNA recognition by *Escherichia coli* replicative helicase DnaB protein. Application of the matrix projection operator technique to analyze stopped-flow kinetics, *J. Mol. Biol. 295*, 831−852.
41. Bujalowski, W., and Jezewska, M. J. (2000) Kinetic mechanism of nucleotide cofactor binding to *Escherichia coli* replicative helicase DnaB protein. Stopped-flow kinetic studies using fluorescent, ribose-, and base-modified nucleotide analogues, *Biochemistry 39*, 2106−2122.
42. Galletto, R., and Bujalowski, W. (2002) Kinetics of the *E. coli* replication factor DnaC protein−nucleotide interactions. II. Fluorescence anisotropy and transient, dynamic quenching stopped-flow studies of the reaction intermediates, *Biochemistry 41*, 8921−8934.
43. Pilar, F. L. (1968) *Elementary Quantum Chemistry*, Chapter 9, McGraw-Hill, New York.
44. Kleinschmidt, C., Tovar, K., Hillen, W., and Porschke, D. (1988) Dynamics of repressor-operator recognition: The Tn10-encoded tetracycline resistance control, *Biochemistry 27*, 1094−1104.
45. Raney, K. D., Sowers, L. C., Millar, D. P., and Benkovic, S. J. (1994) A fluorescence-based assay for monitoring helicase activity, *Proc. Natl. Acad. Sci. U.S.A. 91*, 6644−6648.
46. Record, M. T., Jr., Anderson, C. F., and Lohman, T. M. (1978) Thermodynamic analysis of ion effects on the binding and conformational equilibria of proteins and nucleic acids: The roles of ion association or release, screening, and ion effects on water activity, *Q. Rev. Biophys. 11*, 103−178.
47. Record, M. T., Lohman, T. M., and deHaseth, P. L. (1976) Ion effects on ligand−nucleic acid interactions, *J. Mol. Biol. 107*, 145−158.
48. Berg, O. G., Winter, R. B., and von Hippel, P. H. (1981) Diffusion-Driven Mechanisms of Protein Translocation on Nucleic Acid. Models and Theory, *Biochemistry 20*, 6929−6948.
49. von Hippel, P. H., and Berg, O. G. (1989) Facilitated Target Location in Biological Systems, *J. Biol. Chem. 264*, 675−678.
50. Lohman, T. M., and Kowalczykowski, S. C. (1981) Kinetics of the Association of the Bacteriophage T4 Gene 32 (Helix Destabilizing) Protein with Single-stranded Nucleic Acids. Evidence for Protein Translocations, *J. Mol. Biol. 152*, 67−109.
51. Lohman, T. M. (1986) Kinetics of protein−nucleic acid interactions: Use of salt effects to probe mechanisms of interaction, *CRC Crit. Rev. Biochem. 19*, 191−245.
52. Lohman, T. M. (1984) Kinetics and mechanism of dissociation of cooperatively bound T4 gene 32 protein-single-stranded nucleic acid complexes. 1. Irreversible dissociation induced by sodium chloride concentration jumps, *Biochemistry 23*, 4656−4665.
53. Porschke, D., and Rauh, H. (1983) Cooperative Excluded-Site Binding and Its Dynamics for the Interaction of Gene 5 Protein with Polynucleotides, *Biochemistry 22*, 4737−4745.
54. Schranner, R., and Richter, P. H. (1978) Rate Enhancement by Guided Diffusion. Chain Length Dependence of Repressor-Operator Association Rates, *Biophys. Chem. 8*, 135−150.
55. Edgerton, M. E., Handler, F. A., and Wu, C.-W. (1983) Methods for the Analysis of the Kinetics of Cooperative Binding of Ligands to a Two-Site Lattice, *Biopolymers 22*, 787−805.
56. Berry, R. S., Rice, S. A., and Ross, J. (1980) *Physical Chemistry*, pp 1117−1204, Wiley, New York.
57. Jezewska, M. J., Galletto, R., and Bujalowski, W. (2003) Rat polymerase β gapped DNA interactions: Antagonistic effects of the 5′ terminal PO^{4-} group and magnesium on the enzyme binding to the gapped DNAs with different ssDNA gaps, *Mol. Cell. Biophys. Biochem. 38*, 125−160.

BI0487037